A machine-learning enhanced analysis of mixed bio-thermal convection of single particle and hybrid nanofluids within a complex configuration

Rasool Alizadeh[1], Javad Mohebbi Najm Abad[2], Abolfazl Fattahi[3], Mehrdad Mesgarpour[4], Mohammad Hossein Doranehgard [5], Qingang Xiong[6,*], Nader Karimi[7,8]

[1]Department of Mechanical Engineering, Quchan Branch, Islamic Azad University, Quchan, 94791-76135, Iran

[2]Department of Computer Engineering, Quchan Branch, Islamic Azad University, Quchan, 94791-76135, Iran

[3]Department of Mechanical Engineering, University of Kashan, Kashan, 87317-53153, Iran

[4]Fluid Mechanics, Thermal Engineering and Multiphase Flow Research Lab. (FUTURE), Department of Mechanical Engineering, Faculty of Engineering, King Mongkut's University of Technology Thonburi (KMUTT), Bangmod, Bangkok 10140, Thailand

[5] Department of Civil and Environmental Engineering, School of Mining and Petroleum Engineering, University of Alberta, Edmonton, Alberta T6G 1H9, Canada

[6] State Key Laboratory of Pulp and Paper Engineering, South China University of Technology, Guangzhou, 510640, China

[7] School of Engineering and Materials Science, Queen Mary University of London, London E1 4NS, United Kingdom

[8] James Watt School of Engineering, University of Glasgow, Glasgow G12 8QQ, United Kingdom

*Corresponding author. Email: qingangxiong@scut.edu.cn (Q. Xiong)

Abstract

Transport phenomena in a hybrid or single-particle nanofluid over a conical body embedded inside a porous medium are investigated. The fluid contains homogenously mixed nanoparticles and alive cells that are able to migrate, collectively sculpturing a thermo-bio-solutal system. Transport processes including mixed convection as well as species and cell transfer are simulated using a similarity technique. As the problem involves a large number of parameters with complicated interactions, machine learning is applied to predict a wide range of parametric variations. The simulation data are used to build an intelligent tool based on artificial neural network to predict the behaviour of the system. This also aids development of precise correlations for non-dimensional parameters dominating the transport phenomena. The results indicate that the lower values of motile Lewis number and higher mixed convection parameter enhance the Nusselt number. However, it is contained respectively by Peclet number increment and increases in the bio Rayleigh number. It is further shown that an increase

in Prandtl number enhances Sherwood number and makes the motile microorganisms more uniform. Peclet number directly influences the transport of heat, mass, and microorganisms. The study clearly demonstrates the abilities of combining numerical simulations with machine learning to significantly extend and enrich analysis of problems with large number of variables. The findings also pave the way for predicting behaviors of complex thermo-bio-solutal systems without resorting to computationally demanding simulations.

Keywords: Bio-thermal convection; Motile microorganisms; Hybrid nanofluid; Artificial Neural Networks; Machine learning

---

Nomenclature

a	Constants	q_m	Mass flux on the wall
A_1, A_2, A_3, A_4, A	Constants	q_n	Motile Microorganisms flux on the wall
a_{sf}	Interfacial area per unit volume of porous media	q_w	Heat flux on the wall
AI	Artificial intelligence	$r(x)$	Cone radius
ANN	Artificial Neural Networks	Re	Freestream Reynolds number
b	Chemotaxic constant	S	Shape factor
Bi	Biot number	Sc	Schmidt number
c	Concentration of nanoparticles	Sh	Sherwood number
C	Non-dimensional concentration of nanoparticles	Sh_m	Average Sherwood number
C_p	Specific heat at constant pressure	T	temperature
D_m	Brownian diffusion coefficient	u, v	velocity in x and y directions
D_n	Microorganisms diffusion	$V_{o,i}$	weights between the bias and the i-th neuron of the hidden layer
f	velocity function in y direction	$V_{i,j}$	weights between the j-th neuron of the hidden layer with i-th neuron of the output layer
f'	velocity function in x direction	W_c	Maximum cell swimming speed
f_i	output of i-th neuron of the hidden layer	$W_{o,i}$	weight between the bias and the i-th neuron of the hidden layer

f_j	output of j-th neuron of the hidden layer	$W_{i,j}$	weight between the j-th neuron of the input layer and i-th neuron of the hidden layer
FCD	F-test correlation difference	x, y	Coordinate axes
g	Gravitational acceleration	x_j	j-th input of the neural network
Gr	Grashof number	**Greek symbols**	
h	Heat transfer coefficient	α	Thermal diffusivity
h_{sf}	Interstitial heat transfer coefficient	β	Thermal expansion Coefficient
$I(x, y)$	MI between two features of x and y	β^*	Solutal expansion Coefficient
k	Thermal conductivity	γ	Average volume of a microorganism
k_1	Permeability of the porous medium	γ^*	the modified conductivity ratio
k_m	Mass transfer coefficient	γ_1	The half cone angle
k_n	Motile Microorganisms coefficient	δ	the bio-convection constant
L	Cone length	ε	Porosity
L_b	the bio-convection Lewis number	η	Similarity variable
MLP	Multi-Layer Perceptron	θ	Non-dimensional temperature
MID	Mutual Information Difference	λ	Permeability parameter
n	density Motile of Microorganisms	λ_1	Dimensionless mixed convection parameter
N	Non-dimensional density Motile of Microorganisms	μ	Dynamic viscosity
N_b	the bio-mix convection Rayleigh number	ν	Kinematic viscosity
N_c	the ratio of concentration to thermal buoyancy forces	ρ	Fluid density
Nu	Nusselt number	ρ_m	Microorganism density
Nn	Density number of Motile Microorganisms	ϕ_1, ϕ_2	Solid volume fraction of nanoparticles 1 and 2.
Nu_m	Average Nusselt number	**Subscripts**	
O_i	weighted output for each neuron of the output layer	f	Fluid

$P(x,y)$	probability density functions based on the variables x, y	hnf	Hybrid nanofluid
Pe	the bio-convection Peclet number	s	Solid
Pr	Prandtl number	w	Related to the external wall of the cone
PSO	Particle Swarm Optimization	∞	Far field

1. Introduction

Biological thermal convection plays a central role in many natural and bio-engineered systems [1-3]. In general, transport of heat and mass in such systems is more complex than that in non-biological systems as the existence of microorganisms can significantly complicate the problem [4-5]. This stems from changing thermo-physical properties of the base fluid by blending nanoparticles as well as reconfiguring the general sculpture of diffusion and convection of the nanofluid by adding microorganisms. [6-7]. Most importantly, exploring such complicated physics is central to the control of the biological systems for reaching high levels of bio-efficiency. Similar to mass conservation for the nanofluid, the cells require their own transport equation [8-9]. In many biological applications, such fluid passes through porous media [10-11]. The resultant problem ends up having a large number of influencing parameters. Given the high sensitivity of biological systems to variations in temperature, heat transfer analysis becomes an essential task. Here, we show that machine learning can be effectively incorporated into an, otherwise, classical study to significantly enhance the predictability of a heat transfer model.

In the followings, first the state of the art in the modelling of heat convection and bio-convection with nanofluids is briefly reviewed and then the use of machine learning in heat transfer analysis is discussed. Devi and Devi [12-13] scrutinized the advantages of the application of hybrid Alumina-copper-water nanofluids over the stretching surface. The rate of heat transfer increased in the presence of hybrid nanofluids. A higher heat transfer rate was achieved by applying hybrid nanofluid in comparison to that of single-particle nanofluid. Lund et al. [14] solved the governing equations for fluid flow and heat transfer of Cu-Fe_3O_4-H_2O hybrid nanofluid in porous media using a similarity transformation method. It was reported that the rate of heat transfer was reduced by applying more copper nanoparticles and plate suction.

Emami et al. [15] numerically investigated the laminar heat convection of Cu-water nanofluid in a porous cavity affected by the inclination angle and heater configuration. It was shown that the application of nanofluid and porous media was beneficial for heat transfer only in the low to moderate natural convection regimes and the strong natural convection was inversely affected by them. The corner positioning of the heater was found to be more influential. El-Shorbagy et al. [16] numerically investigated the convective heat transfer of a nanofluid in a trapezoidal porous channel. Permeability and Darcy number showed a non-conventional trend. The Nusselt number depicted increasing-

decreasing variation by the height of the channel. The heat transfer and fluid flow in a V-shaped cavity of heterogeneous, partially layered porous material was numerically investigated by Raizah et al. [17]. The horizontal positioning of the porous layer was identified as the optimal thermal case.

Chao [18] investigated the effects of combining porous media with nanofluid on natural convection in a wavy wall cavity. By intensifying the volume fraction of the nanoparticles and amplitude of the wave, Bejan and Nusselt number rose and entropy generation was mitigated. Increasing the porosity, Nusselt number, volume fraction of nanoparticles, and Rayleigh number made a significant augmentation of heat transfer. The mixed convection of the hybrid Cu-Alumina-water nanofluid was assessed in a trapezoidal cavity by Cimpean et al. [19]. Reynolds and Darcy number increment led to heat transfer enhancement. Kadhim et al. [20] conducted a parametric study of natural convection heat transfer in an inclined cavity configured with two opposing wavy walls and saturated with layered porous medium and hybrid nanofluid of Cu-Alumina-water. The aiding or destroying contribution of porous media in heat transfer depended on the inclination angle. Golamalipour et al. [21] investigated the effects of eccentricity of an annular heat source in a porous cavity contained Cu-water nanofluid and concluded that the downward settling of the heat source made the heat transfer to be the most enhanced and entropy generation negligible.

Khademi et al. [22] studied mixed convection of a nanofluid on a plate in a porous medium and reported that Richardson number affected the nanoparticles dispersion level. The laminar forced convection in a U-turned pipe filled with hybrid nanofluid and the porous medium was investigated by Moghadasi et al. [23]. Increasing Darcy number provoked the performance evaluation criteria to increase while thickening the porous media intensified the pressure drop. Waini et al. [24] considered mixed convection over a flat plate that emerged in a porous media, while a hybrid nanofluid of Cu-Alumina-water was passed on. The similarity solution showed applying hybrid nanoparticles was beneficial to postpone the boundary layer separation. The same hybrid nanofluid was used by Ahmed [25] in the analysis of mixed convection of an inclined porous cavity using the fractional derivative method. The parameters were divided into two main categories, as those made opposing or aiding flow pattern. Bari [26] evaluated nanofluid free convection in a porous medium, aiming to cool an electrical device. A general correlation for the Nusselt number was introduced. The volume ratio of porous material matrix to that of the base fluid was found an outstanding parameter affecting heat transfer. Sheikholeslami [27] numerically simulated a 3D porous cavity filled with a nanofluid and showed the straight relation between heat transfer and non-dimensional numbers of Reynolds and Darcy number. A similar relation was introduced for the kinetic energy of the nanofluid.

Chamkha et al.[28-30] studied free convection and mass transfer from a vertical cone with magnetic field and heat generation and radiation effects. They are found that the local tangential and skin-friction coefficients and local Nusselt and Sherwood numbers increase with the time when the angular velocity of the cone increases, but the reverse trend is observed for decreasing angular velocity. The mixed convection flow and mass transfer with a magnetic field was investigated by Takhar et al.[31-32]. The

results indicate that the magnetic field significantly affects the velocity components and these, in general, decrease with an increasing magnetic field, whereas the temperature increases.

The bio-convection heat transfer using nanomaterials has been repeatedly found in the literature more than ever since firstly introduced by Platt [33]. The bio-convection heat transfer involves many applications in systems involving alive cells where heat transfer enhancement and high mass mixing are sought. It can be triggered by floating the low-density microorganisms in a liquid, specified by patterns in the cell mitigation [2], due to inherent fluctuations [34].

Kuznetsov [35] depicted patterns of the bio-convection forming in nanofluid suspension. He sought to solve the stability problem using the Galerkin method to model geophysical and sedimentary applications. In other studies, this author [36-37] conducted the convection of a nanofluid including nanoparticles and motile microorganisms. The model considers Brownian motion and thermophoresis effects. The results showed that the heated zone location on the boundaries and the Rayleigh number of the nanofluid without microorganisms could considerably destabilize the suspension [36]. Saini and Sharma [38] stepped forward by considering more realistic boundary conditions in the bio-thermal convection problem. The combined presence of thermophoresis, Brownian motion, and microorganisms made a decreasing effect on the thermal Rayleigh number and destabilizing the flow. However, heart transfer was on the enhancement for microorganisms' convection. They also performed a linear and non-linear stability analysis of bio-thermal convection [39]. The effect of bio-convection on the thermal convection was found as a function of Peclet number [39]. Lewis number and nanoparticles Rayleigh number induced larger-scale cells [40].

Bio-convection over a flat surface was analyzed using a similarity method by Xu [41]. Zaimi et al. [42] analytically assessed the bio-convection of stagnation flow over a stretching-sucking plate. The suction resulted in a higher local Nusselt number and microorganism density. Xu and Pop [43] investigated the mixed convection in a fluid flow suspended by both nanoparticles and microorganisms. The application of the passive method to solve the problem was broadly discussed. Using a similarity solution, the bio-convection on a horizontal flat plate surrounded by porous material and submerged in the nanofluid and microorganisms was investigated by Beg et al. [44]. Lewis number led to enhanced nanoparticle concentration and elevate density function of the microorganisms. Kumar et al. [45] studied the Stagnation point problem under slip conditions of velocity and heat transfer considering a mixed-convection. By conducting an unsteady solution, Peclet number augmentation diminished microorganisms' concentration. Increment of the mixed convection parameter had a suppressing effect on heat transfer and motile microorganism transfer.

Application of machine learning (ML) for prediction purpose is growing rapidly in many areas leaving a profound impact on various engineering and scientific fields [46]. This method has been shown to be most useful for the analysis of computationally expensive problems, see for example [47-48]. By developing hard and soft reservoirs of computing machines, ML has become a vital complement for experimental, computational, and theoretical fluid dynamics [49- 50]. In recent years, some research have

been performed on using machine learning together with computational fluid dynamics (CFD) problems [51-55]. This predictive tool can significantly push the boundaries of classical approaches and allows conduction of more sophisticated analysis.

The current study conducts an analytical-numerical investigation of the bio-thermal mixed convection of a hybrid nanofluid in a porous medium containing a conical geometry. Such configuration has been rarely investigated in the past. As the problem contains the impact of many variables including Prandtl number, Peclet number, Rayleigh number, Lewis number, motile density number, mixed convection parameter, and others on the heat, mass, and cells transfer, ML is a beneficial computing predictor to subside the number of simulations and to generalize the results. The results, therefore, dominate the whole range of variations for governing independent parameters.

2. Problem description, assumptions, and governing equations

In this study, a mixed bio-convection heat transfer of an embedded cone in a porous medium is investigated. Fig. 1 shows the geometry of the current problem that is the nanofluid stagnation flow over a conical body embedded in a porous material. The half cone angle is named γ_1.

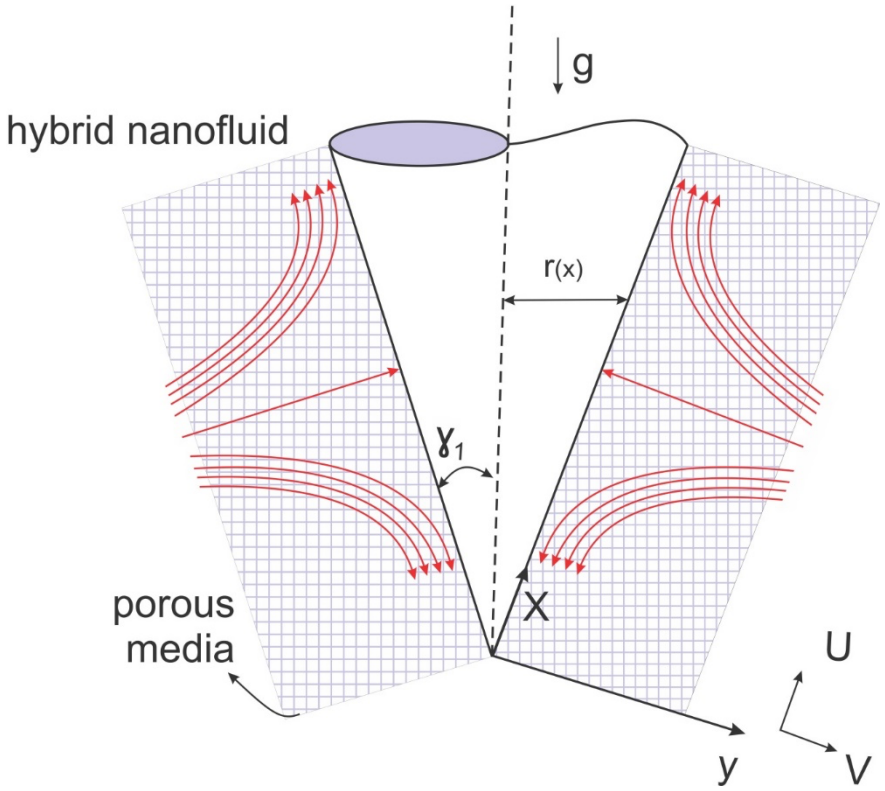

Fig. 1. The Schematic view of a stationary cone under radial stagnation flow in porous media.

The nanofluid is assumed to be Newtonian and single-phase. The thermo-physical properties of the nanofluid are kept at constant values, except by varying the volume fractions of nanoparticles. The fluid flow is assumed to be steady, incompressible, laminar, and the viscous heating of the flow is ignored. The porous medium is homogenous and isotropic with non-equilibrium thermal conditions. It

is further assumed that the porous media cannot absorb the microorganisms and they can easily pass through the pores. Besides, Reynolds number values of the porous medium were assumed to be low so the non-linear effects can be ignored. The hot surfaces are assumed to be maintain at the thermal conditions consistent with requirements of the living microorganisms. The governing equations for the current problem are introduced in the followings.

The continuity equation is

$$\frac{\partial(ru)}{\partial x}+\frac{\partial(rv)}{\partial y}=0; \tag{1}$$

u and v are the velocities in directions x and y shown in Fig.1. The momentum equation in the axial direction takes the form of [56-60]

$$\begin{aligned}\frac{\rho_{hnf}}{\varepsilon^2}\left(u\frac{\partial u}{\partial x}+v\frac{\partial u}{\partial y}\right)&\\ =\frac{\mu_{hnf}}{\varepsilon}\left(\frac{\partial^2 u}{\partial y^2}\right)&\\ +\left\{\mp g.(\rho.\beta)_{hnf}\left[T_f-T_\infty\right]-g.\beta^*(\rho)_{hnf}[c-c_\infty]\right.&\\ \left.-g.\gamma.\left(\rho_m-\rho_{hnf}\right)[n-n_\infty]\right\}\cos\gamma_1-\frac{\mu_{hnf}}{k_1}u.&\end{aligned} \tag{2}$$

In Eq. (2), the subscript hnf denotes the hybrid nanofluid, c is the mass concentration. k_1, ε and n are respectively permeability of the porous medium, porosity, and density of motile microorganisms. Subscripts f, ∞ and m stand for the fluid, far-field, and microorganisms, respectively. In the current study, the flow velocity remains low and therefore the non-Darcy effects have been ignored. The two-equation model is widely employed to model and simulate the LTNE effects. In the two-equation model, the fluid energy conservation equation is written as

$$u\frac{\partial T_f}{\partial x}+v\frac{\partial T_f}{\partial y}=\alpha_{hnf}\left(\frac{\partial^2 T_f}{\partial y^2}\right)+\frac{h_{sf}\,.\,a_{sf}}{\left(\rho.C_p\right)_{hnf}}\left(T_s-T_f\right), \tag{3}$$

where by h_{sf}, α, a_{sf} and C_p show correspondingly the interstitial heat transfer coefficient, thermal diffusivity, interfacial area of the porous media, and heat capacity. Further, subscript s indicates solid media. The thermal energy transport in the solid phase of the porous medium is expressed as

$$k_s\left(\frac{\partial^2 T_s}{\partial x^2}+\frac{\partial^2 T_s}{\partial y^2}\right)-h_{sf}\,.\,a_{sf}\left(T_s-T_f\right)=0. \tag{4}$$

The advective-diffusive model is applied to represent the mass transfer of nanoparticles [13, 61] that is

$$u\frac{\partial c}{\partial x}+v\frac{\partial c}{\partial y}=D_m\left(\frac{\partial^2 c}{\partial y^2}\right), \tag{5}$$

where D_m is the mass diffusivity coefficient of microorganisms. The cell conservation transport for the microorganisms is depicted by[36-37]

$$u\frac{\partial n}{\partial x}+v\frac{\partial n}{\partial y}+\frac{b.W_c}{c_w-c_\infty}\frac{\partial}{\partial y}\left[n\frac{\partial c}{\partial y}\right]=D_n\left(\frac{\partial^2 n}{\partial y^2}\right), \quad (6)$$

in which b and W_c illustrates chemotaxis constant and the maximum speed of cells swimming, individually. Corresponding to Eq. (6), the cell's transport can be performed by fluid convection, self-sustained swimming and diffusion [35]. The boundary conditions used for solving the preceding governing equations can be written as follows.

- No-slip condition on the cone wall and far filed velocity function lead to the following equations.

$$y=0: \quad u=0\,,\ v=0, \quad (7)$$

$$y=\infty: \quad u=ax\,,\ v=ay. \quad (8)$$

Eq. (8) illustrates that the potential flow is approached by tending "y" to infinity [33-34].

- The boundary conditions for the energy equation can be written as:

$$\begin{aligned} y=0: \quad & T_f=T_w=\text{Constant},\\ & T_s=T_w=\text{Constant},\\ y=\infty: \quad & T_f=T_\infty,\\ & T_s=T_\infty, \end{aligned} \quad (9)$$

where T_w and T_∞ show the cone wall and ambient temperature, respectively.

- Finally, the boundary conditions for solute transport are represented by:

$$\begin{aligned} y=0: \quad & c=c_w,\\ y=\infty: \quad & c\to c_\infty, \end{aligned} \quad (10)$$

in which c_∞ stands for the concentration in the free-stream.

The boundary conditions of cell conservation are also required. These are

$$\begin{aligned} y=0: \quad & n=n_w\\ y=\infty: \quad & n\to n_\infty \end{aligned} \quad (11)$$

3. Numerical and theoretical methods

3.1. Self-similar solutions

The following similarity transformations were applied for reducing the governing equations to be solved more readily.

$$u=a.x.f'(\eta), \qquad v=-\sqrt{a.\upsilon}\,.f(\eta), \quad (12)$$

where $\eta=\sqrt{\frac{a}{\upsilon}}y$ is defined as the non-dimensionless radial variable. By applying this transformation, the non-dimensional differential equation of momentum is obtained as

$$\varepsilon f'+A_1.A_2[ff'-(f')^2]+\varepsilon^2.A_1\{\pm A_5.\lambda_1.\theta_f-N_c.C-N_b.N\}+\varepsilon^2.\frac{\lambda}{Re}f'=0, \quad (13)$$

whereby $Re=\frac{a.L^2}{\upsilon_f}$ stands for Reynolds number of free stream and $\lambda=\frac{L^2}{k_1}$ is defined as the permeability parameter (permeability parameter is the inverse of Darcy number). The dimensionless mixed

convection parameter is shown by $\lambda_1 = \frac{Gr}{Re^2} = \frac{g.\beta_f\left(T_w - T_\infty\right)\cos\gamma_1}{L.a^2}$ and the ratio of concentration to thermal buoyancy forces is depicted by $N_c = \frac{g.\beta^*.\rho_f.\left(c_w - c_\infty\right)\cos\gamma_1}{L.a^2}$. Further, $N_b = \frac{g.\gamma.\Delta\rho.(n_w - n_\infty)\cos\gamma_1}{L.a^2}$ denotes the bio-mix convection Rayleigh number. The constants A_i are described later. The prime sign in Eq. (13) shows the derivative with respect to η. The boundary conditions for the last equation can be obtained as

$$\eta = 0: \qquad f'(0) = 0 \qquad f(0) = 0, \tag{14}$$

$$\eta \to \infty: \qquad f'(\infty) = 1 \tag{15}$$

Applying the transformation in Eq. (16) to the energy equation results in the following equation [35, 36],

$$\theta_f(\eta) = \frac{T_f(\eta) - T_\infty}{T_w - T_\infty}, \tag{16}$$

$$\theta'_f + \frac{A_3}{A_4} Pr.\left(f.\theta'_f\right) + \frac{Bi}{Re}.\frac{1}{A_4}\left(\theta_s - \theta_f\right) = 0, \tag{17}$$

where Pr and Re represent Prandtl and Reynolds number. Further, Biot number is illustrated by $Bi = \frac{h_{sf} a_{sf}.a}{4k_f}$. Reduced thermal boundary conditions read

$$\begin{aligned} &\eta = 0: \qquad \theta_f(0) = 1, \\ &\eta \to \infty: \qquad \theta_f(\infty) = 0. \end{aligned} \tag{18}$$

Transformation of energy transport of solid phase and its boundary conditions using Eq. (16) gives

$$\theta'_s - \frac{Bi.\gamma^*}{Re}\left(\theta_s - \theta_f\right) = 0, \tag{19}$$

$$\begin{aligned} &\eta = 0: \qquad \theta_s(0) = 1, \\ &\eta \to \infty: \qquad \theta_s(\infty) = 0. \end{aligned} \tag{20}$$

The value of $\gamma^* = \frac{k_f}{k_s}$ in Eq. (19) stands for the modified conductivity ratio.

Similar to temperature in the energy equation, the following transformation forms of mass concentration are applied to reduce the mass transport equation.

$$C(\eta) = \frac{c(\eta) - c_\infty}{c_w - c_\infty}. \tag{21}$$

The dimensionless form of the equation sought is written as.

$$C' + Sc[f.C'] = 0, \tag{22}$$

in which, the Schmidt number is depicted as $Sc = \frac{\upsilon_f}{D_m}$. This equation can be solved by the following transformed boundary conditions

$$\begin{aligned} &\eta = 0: \qquad C(0) = 1, \\ &\eta \to \infty: \qquad C(\infty) = 1 \end{aligned} \tag{23}$$

The dimensionless variable for reducing the cell conservation, Eq. (6), is expressed by

$$N(\eta) = \frac{n(\eta) - n_\infty}{n_w - n_\infty}. \tag{24}$$

After Substitution of Eqs. (12) and (24) into Eq. (6), the cell conservation equation and its boundary conditions are given as

$$N' + Pr.L_b[f.N'] + P_e\left[N'.C' + C'^{(N+\delta)}\right] = 0, \tag{25}$$

$$\eta = 0: \quad N(0) = 1, \tag{26}$$

$$\eta \to \infty: \quad N(\infty) = 0,$$

in which $L_b = \frac{\alpha_f}{D_n}$, $\delta = \frac{n_\infty}{n_w - n_\infty}$ and $P_e = \frac{b.W_c}{D_n}$ indicate the bio-convection Lewis number, the bio-convection constant, and the bio-convection Peclet number, respectively.

The constants A_1, A_2, A_3, A_4 and A_5 in Eqs. (13) and (17) are defined as

$$A_1 = (1-\phi_1)^{2.5}(1-\phi_2)^{2.5},$$

$$A_2 = (1-\phi_2)\left[(1-\phi_1) + \phi_1\left(\frac{\rho_{s_1}}{\rho_f}\right)\right] + \phi_2\left(\frac{\rho_{s_2}}{\rho_f}\right),$$

$$A_3 = (1-\phi_2)\left[(1-\phi_1) + \phi_1\frac{(\rho.C_p)_{s_1}}{(\rho.C_p)_f}\right] + \phi_2\frac{(\rho.C_p)_{s_2}}{(\rho.C_p)_f}, \tag{27}$$

$$A_4 = \frac{k_{s_1} + (s-1)k_f - (s-1)\phi_1(k_f - k_{s_1})}{k_{s_1} + (s-1)k_f + \phi_1(k_f - k_{s_1})}.\frac{k_{s_2} + (s-1)k_{bf} - (s-1)\phi_2(k_{bf} - k_{s_2})}{k_{s_2} + (s-1)k_{bf} + \phi_2(k_{bf} - k_{s_2})},$$

$$A_5 = (1-\phi_2)\left[(1-\phi_1) + \phi_1\frac{(\rho.\beta_t)_{s_1}}{(\rho.\beta_t)_f}\right] + \phi_2\frac{(\rho.\beta_t)_{s_2}}{(\rho.\beta_t)_f}.$$

An implicit, iterative finite-difference method was applied to solve the above equations along with their boundary conditions, as applied in similar studies [37,45]. The convergence criterion was set to 10^{-7} for all governing equations. Being the difference between two consecutive residuals below 10^{-7}, the procedure was terminated and deemed converged. The second-order discretization scheme was applied for transformations of equations in this work.

3.2. Non-dimensional numbers

The role of assessing the transport phenomena in the current study was performed by some non-dimensional variables. Nusselt (Nu) and Sherwood (Sh) numbers show the extent of heat and mass transfer, respectively. Nu on the surface of the cone is obtained from the local convection heat transfer coefficient (h) or the rate of fluid heat transfer (q_w) defined by:

$$h = \frac{q_w}{T_w - T_\infty} = \frac{-k_{hnf}\left(\frac{\partial T_f}{\partial y}\right)_{y=0}}{T_w - T_\infty} = -\frac{k_{hnf}}{x}\frac{\partial \theta_f(0)}{\partial \eta}, \tag{28}$$

$$q_w = -\frac{k_{hnf}}{x}\frac{\partial \theta_f(0)}{\partial \eta}T_w - T_\infty. \tag{29}$$

Therefore,

$$Nu = \frac{h.x}{k_f} = -Re^{\frac{1}{2}}.\frac{k_{hnf}}{k_f}\theta'_f(0) = -A_4.\theta'_f(1) \tag{30}$$

$$Nu.Re^{-\frac{1}{2}} = -A_4.\theta'_f(0). \tag{31}$$

The mass transfer coefficient and its rate can be similarly calculated by

$$k_m = \frac{q_m}{(c_w - c_\infty)} = \frac{-D_m\left(\frac{\partial c}{\partial y}\right)_{y=0}}{(c_w - c_\infty)} = -\frac{D_m}{x}\frac{\partial C(0)}{\partial \eta}, \tag{32}$$

$$q_m = -\frac{D_m}{x}\frac{\partial C(0)}{\partial \eta}C_w - C_\infty. \tag{33}$$

From which Sh is defined as

$$Sh.Re^{-\frac{1}{2}} = \frac{k_m.x}{D_m} = -C'(0). \tag{34}$$

Similarly, the local cell conservation coefficient and rate of cell conservation are indicated as

$$k_n = \frac{q_n}{(n_w - n_\infty)} = \frac{-D_n\left(\frac{\partial n}{\partial y}\right)_{y=0}}{(n_w - n_\infty)} = -\frac{D_n}{x}\frac{\partial N(0)}{\partial \eta}, \tag{35}$$

and

$$q_n = -\frac{D_n}{x}\frac{\partial N(0)}{\partial \eta}N_w - N_\infty. \tag{36}$$

Hence, similar to Nusselt number, the density number of motile microorganisms can be expressed as

$$Nn.Re^{-\frac{1}{2}} = \frac{k_n.x}{D_n} = -N'(0). \tag{37}$$

3.3. Nanofluid properties

In this study, hybrid nanofluid containing CuO nanoparticles and carbon nanotubes (CNTs) in water base fluid is used. Different volume fractions of CuO (ϕ_1) were mixed into the constant 0.1% volume fraction of CNTs (ϕ_2). The thermophysical characteristics of the single-type nanoparticle (Cu) nanofluid and the hybrid Cu-CNTs-water nanofluid can be calculated through the equations represented in Table 1.

Table 1. Thermo-physical properties of the single-type nanoparticle and hybrid nanofluid[53].

Property	Single-type nanoparticle nanofluid	Hybrid nanofluid
Density	$\rho_{nf} = \rho_f\left[(1-\phi) + \phi\left(\frac{\rho_s}{\rho_f}\right)\right]$	$\rho_{hnf} = \rho_f(1-\phi_2)\left[(1-\phi_1) + \phi_1\left(\frac{\rho_{s_1}}{\rho_f}\right)\right] + \phi_2\rho_{s_2}$
Heat capacity	$(\rho.C_p)_{nf} = (\rho.C_p)_f\left[(1-\phi) + \phi\frac{(\rho.C_p)_s}{(\rho.C_p)_f}\right]$	$(\rho.C_p)_{hnf} = (\rho.C_p)_f(1-\phi_2)\left[(1-\phi_1) + \phi_1\frac{(\rho.C_p)_{s_1}}{(\rho.C_p)_f}\right] + \phi_2(\rho.C_p)_{s_2}$
Viscosity	$\mu_{nf} = \frac{\mu_f}{(1-\phi)^{2.5}}$	$\mu_{hnf} = \frac{\mu_f}{(1-\phi_1)^{2.5}(1-\phi_2)^{2.5}}$

Thermal conductivity	$\frac{k_{nf}}{k_f} = \frac{k_s + (s-1)k_f - (s-1)\phi(k_f - k_s)}{k_s + (s-1)k_f + \phi(k_f - k_s)}$	$\frac{k_{hnf}}{k_{bf}} = \frac{k_{s_2} + (m-1)k_{bf} - (m-1)\phi_2(k_{bf} - k_{s_2})}{k_{s_2} + (m-1)k_{bf} + \phi_2(k_{bf} - k_{s_2})}$ $\frac{k_{bf}}{k_f} = \frac{k_{s_1} + (s-1)k_f - (s-1)\phi_1(k_f - k_{s_1})}{k_{s_1} + (s-1)k_f + \phi_1(k_f - k_{s_1})}$

The parameters s and m are called correspondingly shape factor and sphericity that become different for various nanoparticles. s_1 and s_2 indicate CNT nanotubes and Cu nanoparticles, individually. More details of the values for different shapes of nanoparticles can be found in Ref.[53]. Table 2 expresses the thermo-physical properties of water, CNT nanotubes, and Cu nanoparticles.

Table 2. Properties of water, CNTs, and Cu nanoparticles[53]

Property	Water	CNTs	Cu
ρ $(\frac{kg}{m^3})$	997	2600	8933
C_p $(\frac{J}{kg.K})$	4180	425	385
k $(\frac{W}{m.K})$	0.6071	6600	400

4. Grid independency and model validation

To obtain trustworthy results from the modelling, the solution independency from the grid size should be investigated. For this reason, Nu and Sh were calculated for various mesh sizes of 51×18, 102×36, 204×72, 408×144 and 816×288, as tabulated in Table 3. The variations of the preceding numbers showed that the difference is not observable between the two last grids. Thus, the final mesh size selected for the modelling procedure was 408×144 to assure a precise simulation. To capture the sharp gradients around the external surface of the cone, a non-uniform grid was used in η-direction. Further, validation was performed by comparing the present derivative of transformation function values and those of Ref. [63, 64] for two nanotube types charted in Table 4. The average disparity for $f''(0)$ and $\theta'(0)$ are respectively 1 and 0.1 percent, on average. The present analytical-numerical approach could predict the results of similar work with high values of permeability and porosity, with an average error lower than one percent, shown in Table 5. These comparisons confirm the ability of the present approach to capture the underlying physics.

Table 3. Grid independency study at $Bi = 0.1, Re = 5.0, \lambda = 10$.

Mesh size	Nu_m	Sh_m
51×18	1.540873	0.588014
102×36	1.499256	0.555648

204×72	1.479155	0.527381
408×144	1.465920	0.467275
816×288	1.465773	0.468014

Table 4. Comparison between the present work and the results of Khan et al [63].

ϕ_1	$f''(0)$				$-\theta'(0)$			
	Khan et al [63]		Present work		Khan et al. [63]		Present work	
	SWCNT	***MWCNT***	***SWCNT***	***MWCNT***	***SWCNT***	***MWCNT***	***SWCNT***	***MWCNT***
0.01	0.33894	0.33727	0.33871	0.33689	1.10553	1.07905	1.10432	1.07811
0.1	0.40811	0.39008	0.40778	0.38988	4.80627	4.27718	4.80356	4.80112
0.2	0.50452	0.46466	0.50349	0.46327	12.30317	10.56783	12.29854	10.15468

Table 5. Comparison between the present work and the results of Gorla [64] in the limit of very large porosity and permeability.

Re	***f***		***θ***	
	Gorla [64]	Present work	Gorla [64]	Present work
0.01	0.12075	0.12051	0.84549	0.84557
0.1	0.22652	0.22659	0.73715	0.73701
1.0	0.46647	0.46683	0.46070	0.46045
10	0.78731	0.78725	0.02970	0.02983

5. Estimator and optimizer algorithms

5.1. Multi-Layer Perceptron (MLP)

Artificial Neural Networks (ANN) are a set of algorithms and computational models, organized based on what is done by the human brain. They can be applied for voice, image and pattern recognition, robotics, clustering, and classification [65-66]. The output parameters of this study were estimated using MLP neural network. Generally, three layers including input, hidden and output layers make the structure of MLP.

For m inputs in a model, m+1 neurons exist in the input layer. The neurons other than the first one, with the value of unity characterizing the bias role, have the responsibility of receiving input data. The n+1 neurons form the hidden layer. Often, multiple steps could be carried out to calculate the appropriate value for n. The first neuron is again biased similar to that at the first layer. The sum of the weighted output of the previous layer is activated by other neurons of this layer through the following equation [51-52:]

$$f_i = g\left(w_{0,i} + \sum_{j=1}^{m} w_{j,i}\, x_j\right), \tag{38}$$

where, $w_{j,i}$ is used to represent the weight between neuron j of the input layer and neuron i of the hidden layer. Also, $w_{0,i}$ is the weight between the bias and the neuron i of the hidden layer. In addition, x_j presents the input j of the network. f_i is the output of neuron i of the hidden layer. Different function forms, such as logarithmic, hyperbolic, and exponential could be applied for the activation function of g. This is also is applied to each neuron of the output layer similar to the hidden layer [51-52].

$$O_i = h\left(v_{0,i} + \sum_{j=1}^{n} v_{j,i}\, f_j\right), \tag{39}$$

in which the $v_{0,i}$ is the weight between bias and neuron i of the output layer. $v_{j,i}$ depicts the weight between the neuron j of the hidden layer and neuron i of the output layer.

The error back propagation algorithm is used to train the network. In training process, the appropriate weights are calculated according to difference between the network output and actual value. In this step, a known data set in which the target value is determined for each input record is used in a supervised learning process. Proper determination of the appropriate network configuration could remarkably influence its performance.

5.1.1. Feature selection based on mutual information

Feature selection is one of the important steps in designing the model in machine learning. It has a great influence on the performance of the model. A method should be selected for feature selection to show the most contribution to the output variables. The minimum-Redundancy Maximum-Relevance (mRMR) algorithm is an appropriate method which can be used for features prioritization. Mutual Information (MI) is one statistical dependency criterion used in this method. In each step of algorithm, mRMR tries to choose the proper feature which has maximum MI with the model output, while has minimum MI with the set of selected features before that [51-53]. The MI between two features of x and y is calculated by following equation:

$$I(x;y) = \iint p(x,y) \log \frac{p(x)}{p(x)p(y)}\, dxdy \tag{40}$$

where, $p(x)$ and $p(y)$ are the probability density functions of features x and y, respectively. $p(x,y)$ shows the simultaneous occurrence of both variables .

For the problem with many features and records, the execution time of the algorithm is too long. To overcome the time complexity, Mutual Information Difference (MID) or F-test correlation difference (FCD) methods could be applied to estimate it. As the MID approach is more appropriate for non-linear problems, it has attracted more attention recently. It is calculated from the following equation [51-53].

$$MID = max_{i\in\varphi(S)}[I(i,h) - \frac{1}{|S_f|}\sum_{j\in S} I(i,j)] \quad (41)$$

In Eq. (41), S_f indicates the set of selected features. Application of MID scheme in feature selection results in both advantages of mRMR method (acceptable estimation) and lowering the computational complexity, higher speed, and reliability.

5.2. Particle Swarm Optimization (PSO)

The PSO algorithm is one of the suitable approaches for intelligent optimization based on the swarm intelligence concept. In fact, this algorithm was proposed by inspiration from the groups of fishes and birds sharing information with each other. The first contribution to the movement of a particle in an iteration is called $pbest$ which relates to the best position of the particle during its movement. The second one, namely $gbest$ indicates the best position earned by the particles swarm, regardless of which one had achieved it.

The velocity of each particle in each iteration can be calculated as follows [51-53].

$$v_i(t+1) = wv_i(t) + c_1r_1[pbest(t) - x_i(t)] + c_2r_2[gbest(t) - x_i(t)]. \quad (42)$$

The parameters i and t denote the particle index and the iteration number, respectively. The particles' position and velocity are shown by x and v. The random values of r_1 and r_2 are generated in each step of algorithm. The values of acceleration coefficients, c_1 and c_2 are between zero and two. Although their values usually are close to two. Finally, the value of w called the inertia coefficient of velocity is specified between 0.8 and 1.2 [65-66].

The particle position, x, is determined from its velocity, v from the following equation,

$$x_i(t+1) = x_i(t) + v_i(t+1). \quad (43)$$

The number of repetitions of the PSO algorithm in an iterative loop depends on the findings with particular conditions.

6. Results and discussion

In this section, the effects of volume fraction of nanoparticles, Biot, Peclet, Lewis, and Rayleigh number on the heat, mass, and microorganism transport are discussed. The results are obtained by resorting to machine learning technique as explained in Section 5. The default values for different parameters involved are presented in Table 6. Further, the predictor correlations for Nusselt, Sherwood, and density of motile microorganisms are provided later.

Table 6. The default value of the parameters chosen to draw the figures.

Parameter	Re	λ_1	ϕ_2	Pr	γ^*	Pe	δ	ϕ_1	S	λ	N_c	Bi	L_b	Sc	N_b
Values	10.0	*1.0*	*0.1*	*1.0*	*1.5*	*0.1*	*0.1*	*0.1*	*3.7*	*10*	*0.1*	*0.1*	*0.1*	*0.1*	*10*

Fig. 2 shows the variation of Nusselt number versus various parameters. Fig. 2a depicts that the convection heat transfer can be augmented by decreasing the value of Lewis number for motile cells (L_b), indicating higher cells' diffusion. It may result from the negative effect of the cells piling up near

the walls on the temperature gradient. The Nusselt number is also boosted by raising the Peclet number and cells' concentration parameter (δ). Increasing Peclet number makes a change similar to what occurs by cell's Lewis number in microorganism's diffusion. By intensifying δ, the difference in the cells concentration through the medium declines, and therefore, the cells migration subsides. It enhances transport phenomena and therefore more heat is transferred [62]. The extent of relative influences of the aforementioned parameters on heat transfer is not comparable. Fig. 2b portrays that the Nusselt number rises as the mixed convection parameter (λ_1) increases, indicating Reynolds number strengthening, which is physically anticipated. The Nusselt number increment is aggravated in the higher value of bio-mixed Rayleigh number (N_b); the parameter that provides higher heat transfer by relaxing the difference between the cells' concentration all over the domain. In contrast, an increment in N_c makes the Nusselt number lower, as it diminishes the concentration difference across the medium and hinders mass transfer and the subsequent heat transfer. Increasing the shape factor by applying nanoparticles with various geometries can lead to a higher Nusselt number, as depicted in Fig. 2c. Further, the volume fraction of both types of nanoparticles leads to the higher value of heat transfer gradually. Alumina concentration seems to intake more improvement in heat transfer than the CNT nanotubes.

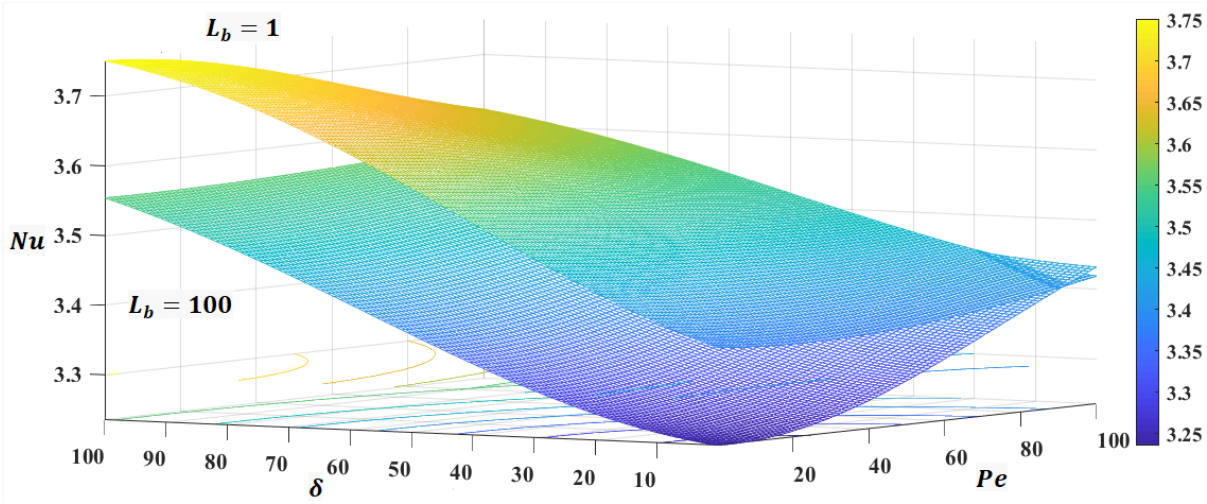

(a)

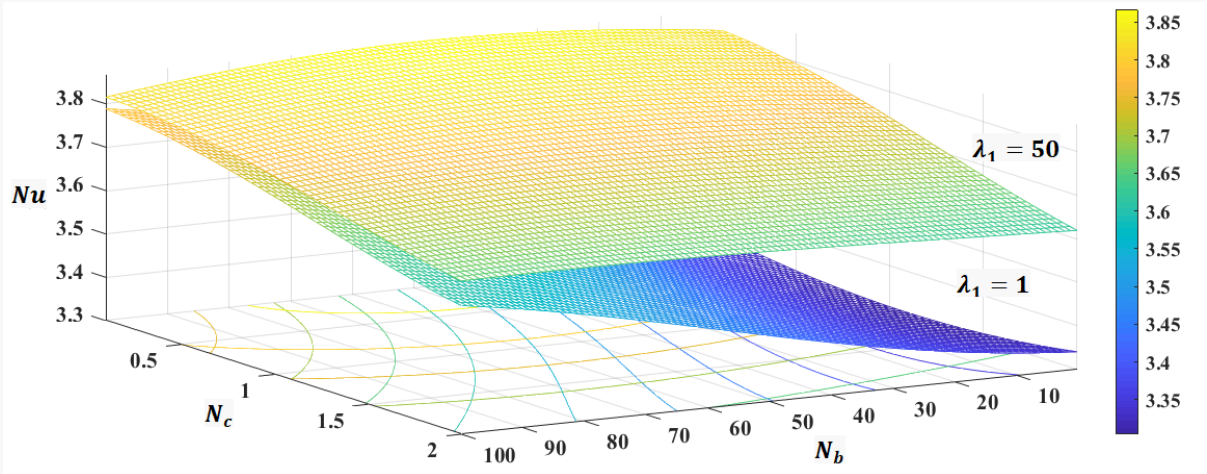

(b)

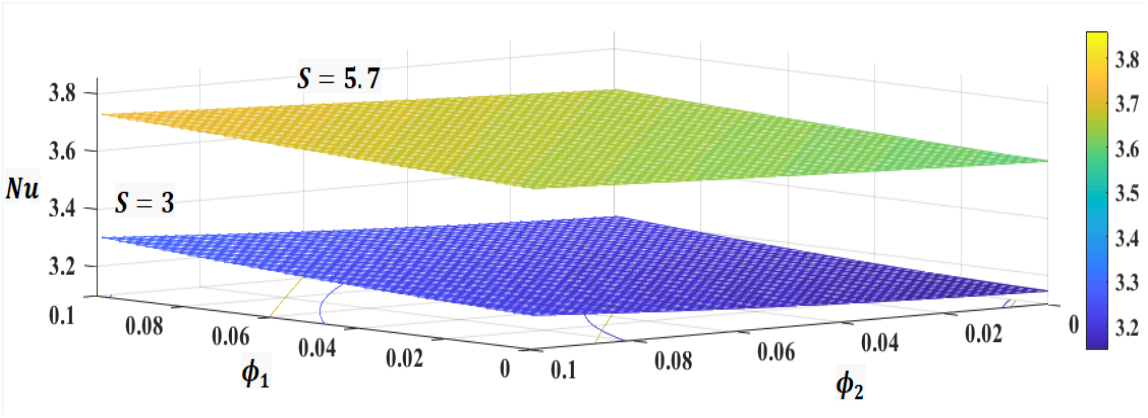

(c)

Fig. 2. Variation of Nu with respect to (a) δ and Pe at two values of bio-convection Lewis number, (b) N_c and N_b at two values of dimensionless mixed convection parameter, and (c) ϕ_1 and ϕ_2 at two values of shape factor.

The Sherwood number variation is plotted in Fig. 3. Subfigure "a" illustrates that a mass transfer drops in a mixture more concentrated with CNT nanoparticles where higher viscosity of nanofluid can harden convective mass transfer. Increasing Prandtl number also has similar impacts. However, the Biot number appears to set a different trend. It is worth noting that the impact of volume fractions on mass transfer may undergo a turning trend in the Prandtl number threshold, which is about 4.5. Decreasing cells' Lewis number boosts the microorganisms' diffusion, which in turn invokes the mass transfer, see Fig. 3b. Increasing the Peclet number increases the swimming velocity of the cells that leads to a higher rates of mass transfer. However, a higher value of δ, which equals to the lower cells' concentration difference through the medium, enhances the transport of mass [45,62]. Subfigure "c" highlights that the mass transfer enhances with strengthening the natural convection or λ_1. The difference between Sherwood number of $\lambda_1 = 1$ and 50 drops if the difference between the cells' concentration (N_b) on the domain becomes larger. Migration of the cells by increasing N_b aids mass transfer, while N_c shows not a remarkable change with variations in Sherwood number.

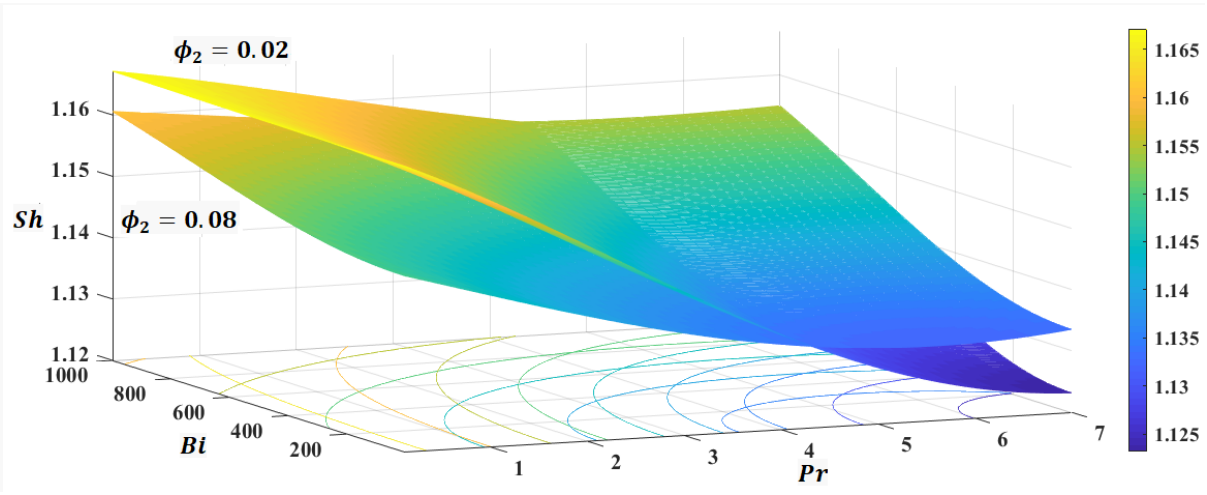

(a)

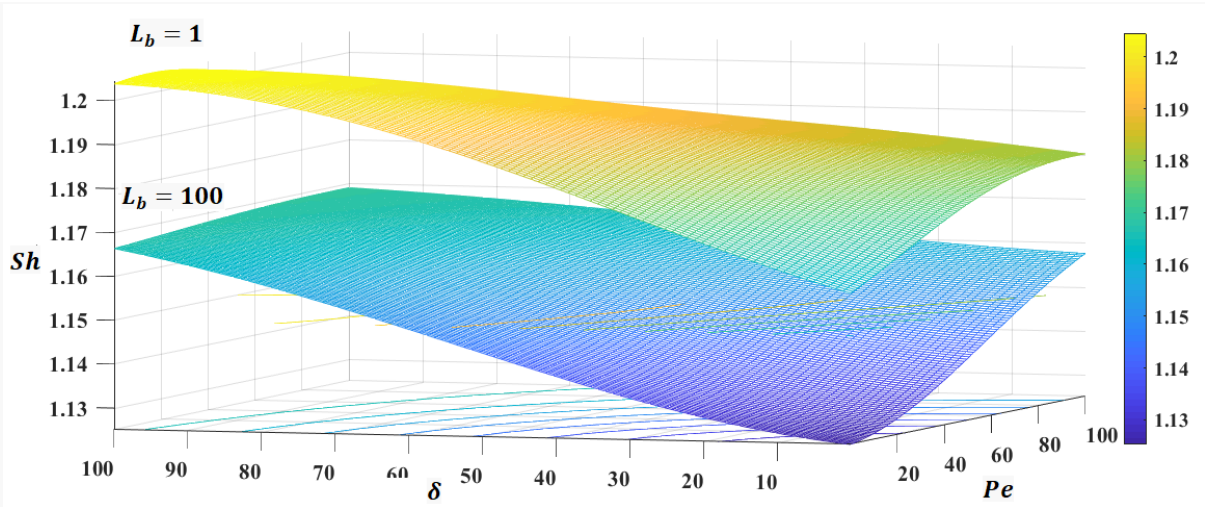

(b)

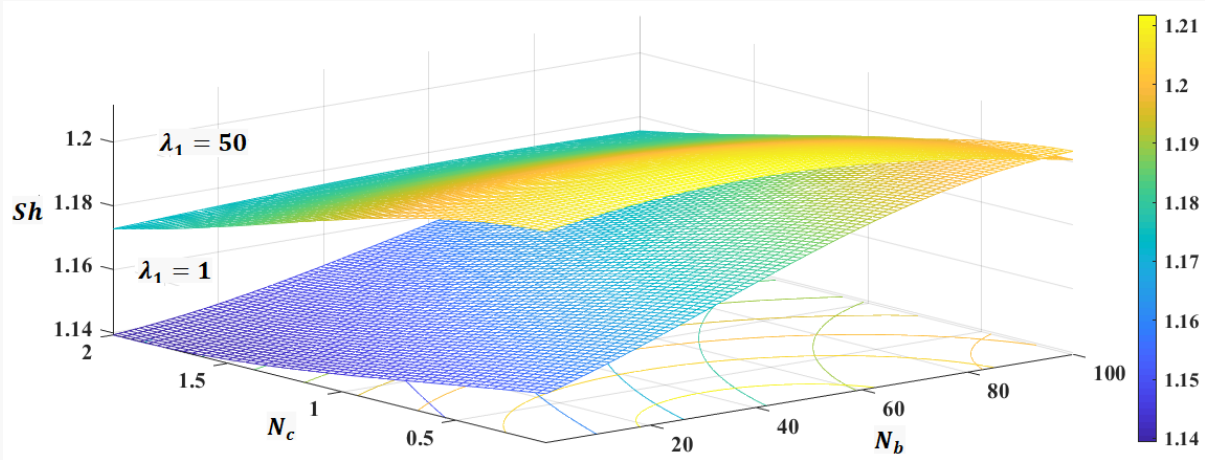

(c)

Fig. 3. Variation of *Sh* with respect to (a) *Bi* and *Pr* at two values of solid volume fraction of nanoparticles, (b) δ and *Pe* at two values of bio-convection Lewis number, (c) N_c and N_b at two values of dimensionless mixed convection parameter.

The density number of motile microorganisms is shown in Fig. 4. Despite no considerable variation, the cells transport is enhanced by increasing the volume fraction of nanotubes, Biot number, or diminishing Prandtl number, shown in Fig. 4a. Lower values of viscosity by dropping Prandtl number aids cells transport. It is found that heat transfer in a concentrated nanofluid pushes more cells to transport, despite increasing the viscosity. However, this trend is contained for lower Prandtl numbers. High values of Biot number overrule the effects of density number by changing ϕ_2. Fig. 4b shows that formation of natural convection recirculation near the body pushes more particles to migrate. This trend turns in $N_b = 70$. Increasing N_b and N_c, delineating a higher difference in cells' concentration and mass concentration, respectively, elevating the level of cells transportation, as expected. Ranging lower than unity, the value of density number indicates the diffusion regime is dominantly determined by the cells motion.

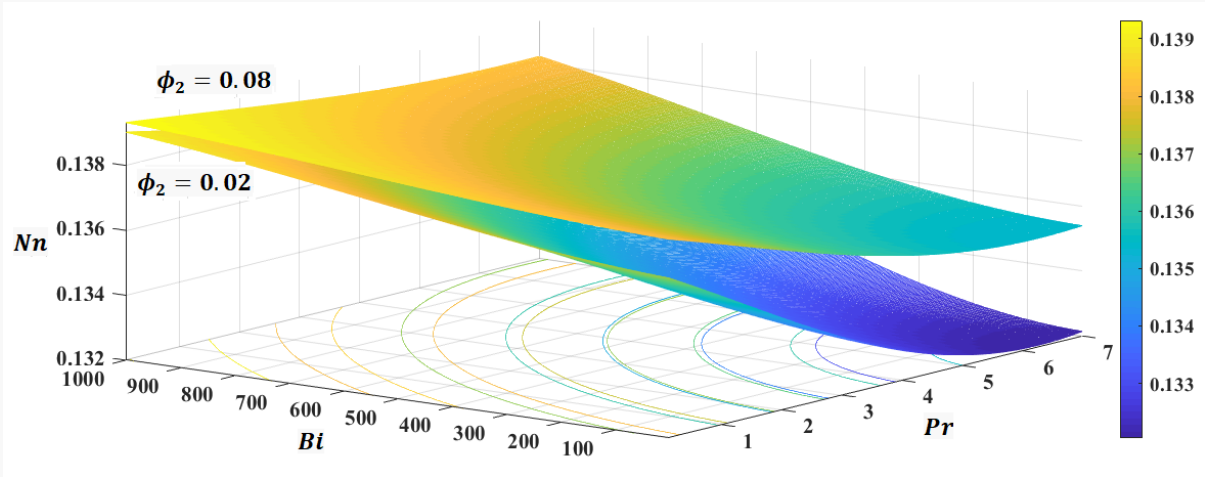

(a)

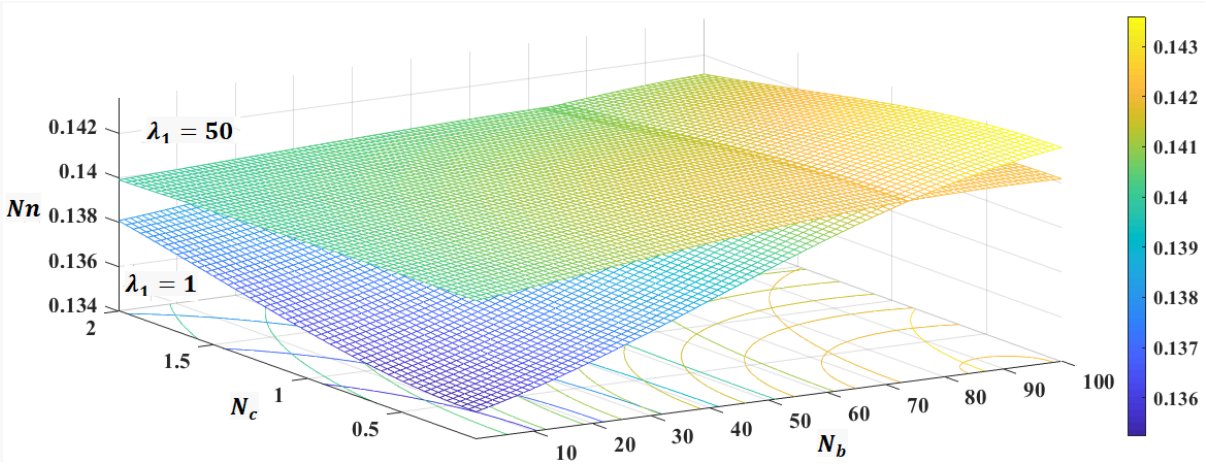

(b)

Fig. 4. Variation of Nn with respect to (a) Bi and Pr at two values of solid volume fraction of nanoparticles, (b) N_c and N_b at two values of dimensionless mixed convection parameter.

Mass concentration variations are demonstrated in Fig. 5. The mass concentration is approached that at the infinity boundary by increasing the momentum diffusivity when Schmidt number is

increased. This stems from boosting momentum forces, as increasing Reynolds number shows a similar effect on the mass concentration. Fig. 5a further expresses that concentration is not affected by changes in Prandtl number. Fig. 5b elucidates that the mass transport is intensified at lower cells' Lewis number; however, its influence is not momentous. Decreasing Peclet number and δ makes higher mass concentration. Therefore, the motile cells migration can drastically affect the mass distribution in the domain.

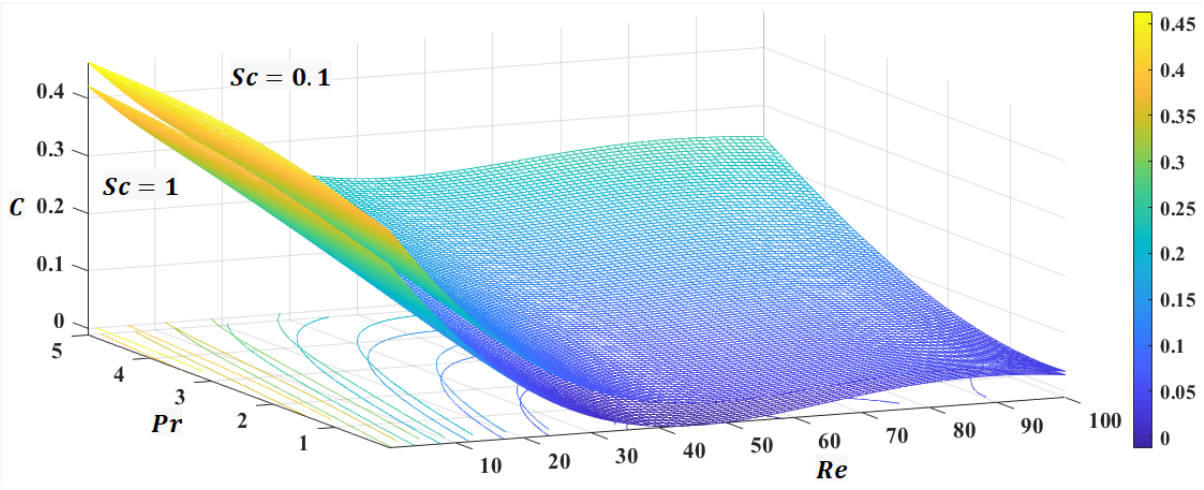

(a)

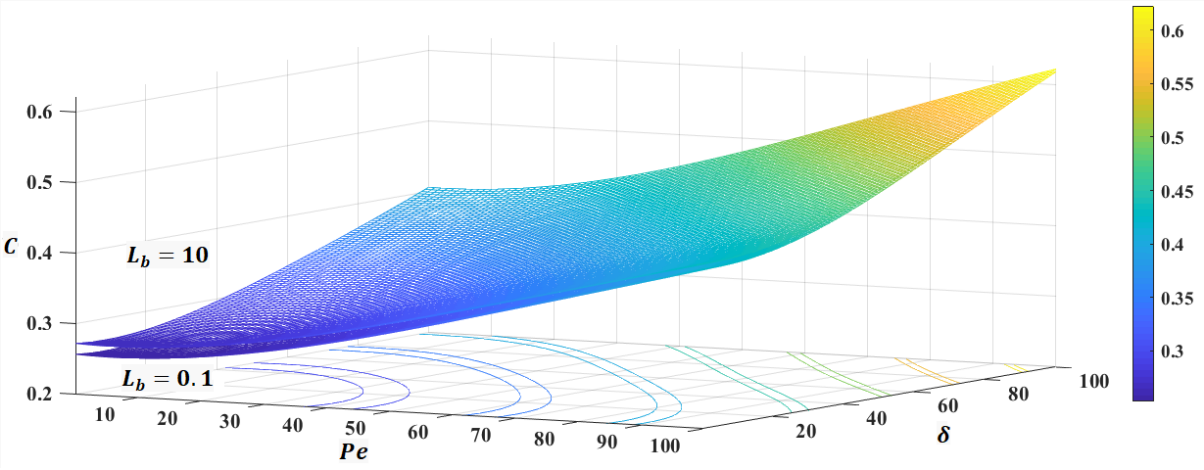

(b)

Fig. 5. Variation of C with respect to (a) Pr and Re at two values of Schmidt number, (b) Pe and δ at two values of bio-convection Lewis number.

The cells concentration is depicted in Fig. 6. Subfigure "a" shows that the higher Reynolds number motivates cells concertation for being close to its value at infinity. It indicates that momentum inertia is a determining parameter to become the cells' density forum uniform. It is accented with considering the trend that makes by the Prandtl number, which its increment weights the momentum diffusivity. A higher volume fraction of nanoparticles also aids higher cells concentration. Fig. 6b indicates cells' Lewis number cannot affect the cells' concentration. However, decreasing Peclet

number, arising from increasing cells' diffusion, invokes the motile concentration being closer to its value at the far boundary. Cell concentration difference $(n - n_\infty)$ undergoes a decreasing pattern by decreasing δ, as expected.

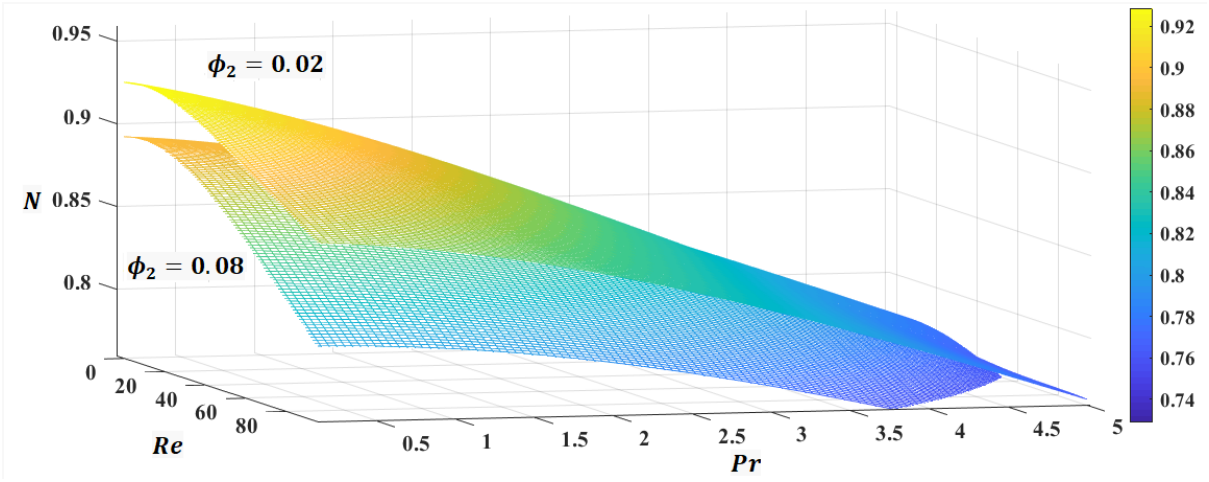

(a)

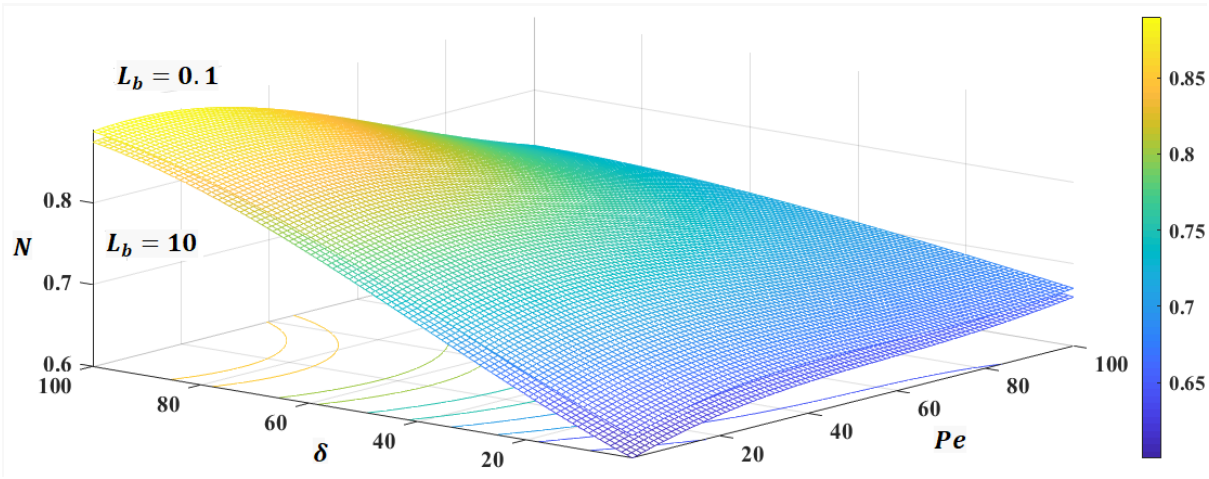

(b)

Fig. 6. Variation of N with respect to (a) Re and Pr at two values of volume fraction of nanoparticles, (b) δ and Pe at two values of bio-convection Lewis number.

As Fig. 7a shows, strengthening the natural convection compared to forced convection helps to be more uniform temperature through the thermal domain. However, the Reynolds number increment, meaning higher forced convection level, can solely upraise the extent of thermal uniformity. Porosity variation through λ seems unlikely to change the temperature distribution. Fig. 7b exhibits that blending more CNT nanotubes in the base fluid turns the temperature to be closer to that at the infinity boundary. Interestingly, the volume fraction of Alumina nanoparticles shows an infinitesimal effect on the temperature domain. Increasing Prandtl number also aids the uniform temperature resulting from increasing thermal conductivity; the way that the nanoparticles create a uniform temperature field.

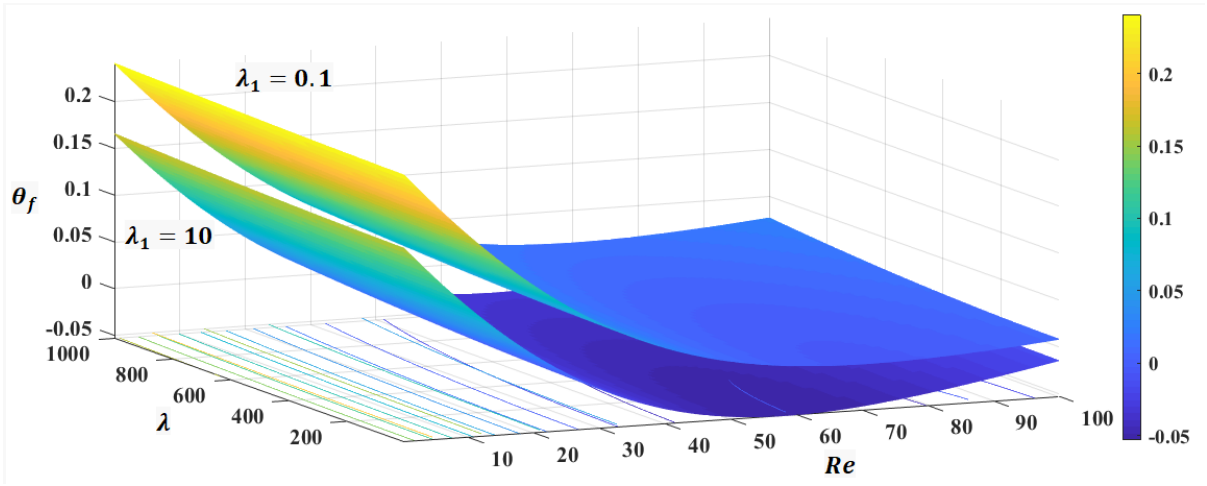

(a)

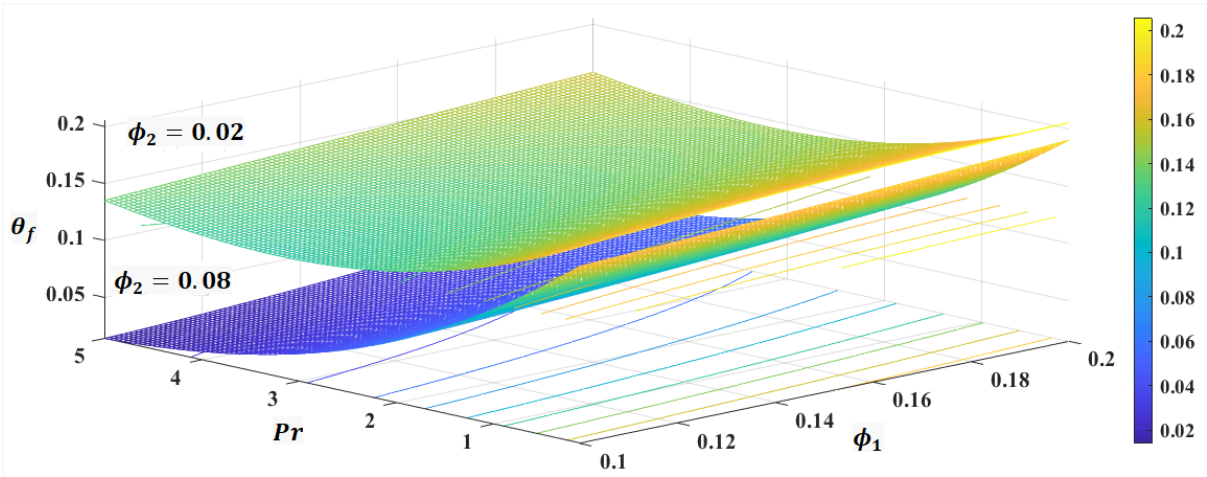

(b)

Fig. 7. Variation of θ_f with respect to (a) λ and Re at two values of dimensionless mixed convection parameter, (b) Pr and ϕ_1 at two values of volume fraction of nanoparticles.

From Fig. 8a, it is perceived that N_c has not influenced the axial velocity. However, increases in the cells' concentration or cone angle through variations in N_b produces larger velocity. It is concluded that the migration of the microorganism cells can be considerably involved in velocity changing. Increasing the cone angle makes more contraction in the fluid passage, resulting in higher velocity. As anticipated, increasing Reynolds number can make a drastic change in the velocity field, following decreasing λ_1. It is confined at low values of N_b. The consequence of increasing the volume fraction of CNT nanotubes is a decrement in axial velocity by boosting the viscosity, portraying by Fig. 8b. The velocity is also an increasing function of porosity, considering λ.

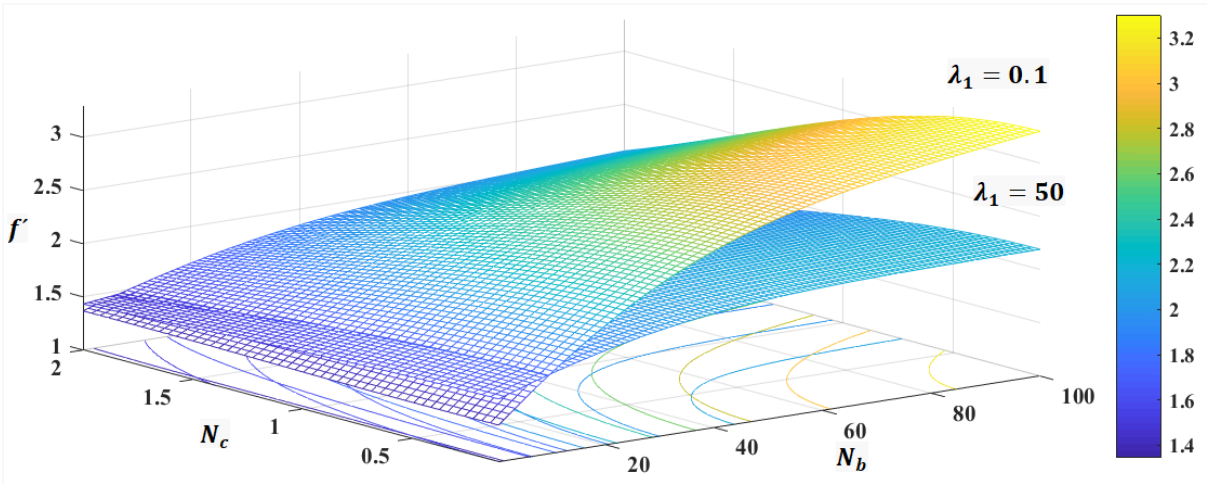

(a)

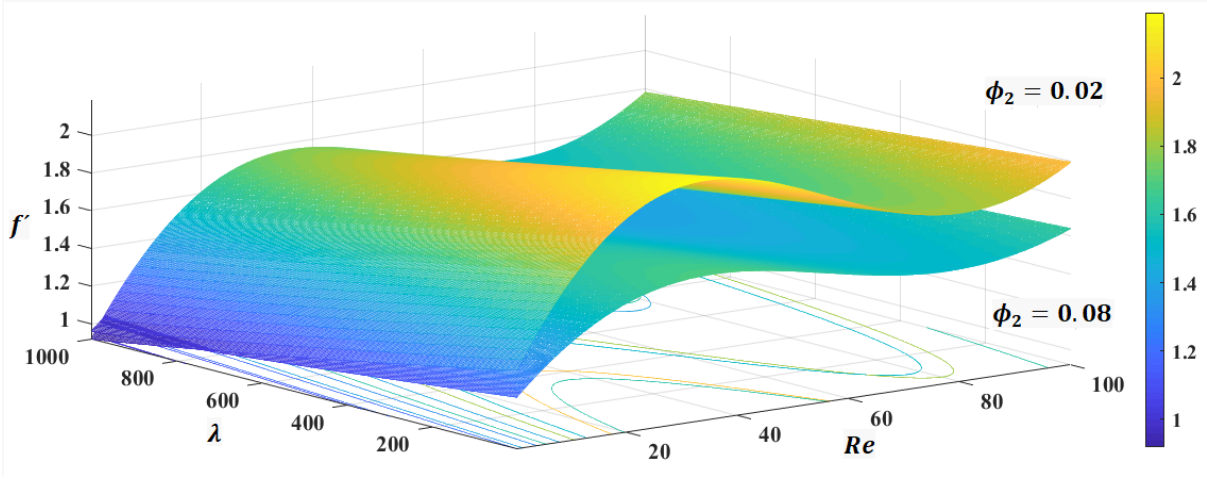

(b)

Fig. 8. Variation of f' with respect to (a) N_c and N_b at two values of dimensionless mixed convection parameter, (b) λ and Re at two values of solid volume fraction of CNT nanotubes.

As visualized by Fig. 9, the solid temperature approaches its infinite boundary value if the thermal conductivity of the solid or fluid mitigates or rises, respectively. Biot number manipulates the solid temperature by making a single-minimum trend, as its complexly contributes to the hydrodynamic and thermal field. This is not the case for Reynolds number that its influence is somewhat negligible.

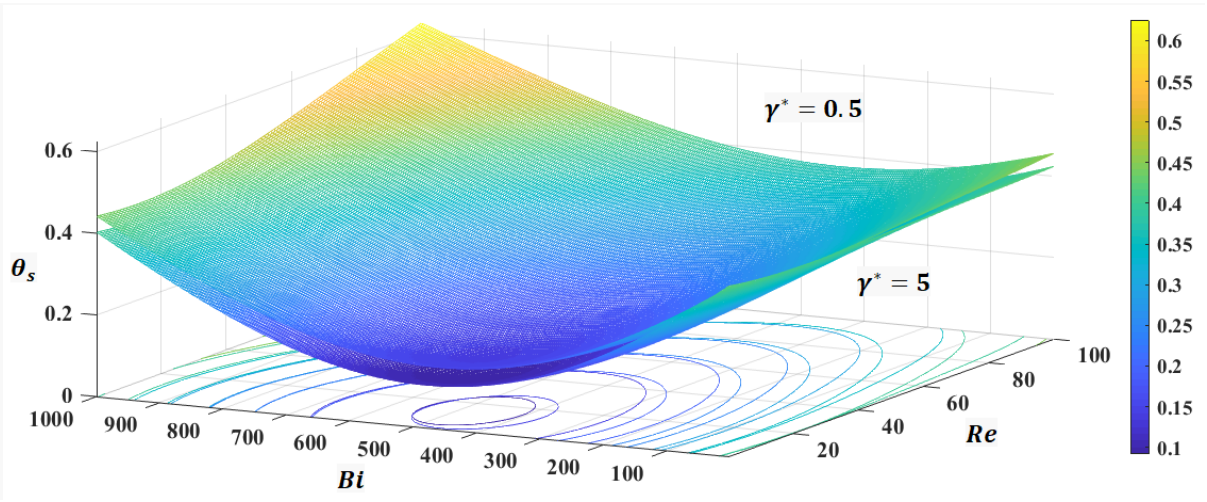

Fig. 9. Variation of θ_s with respect to *Bi* and *Re* at two values of modified conductivity ratio.

Tables 7-9 show the predictors for non-dimensional numbers of Nusselt, Sherwood, and microorganism density number that are the measure for evaluating the relative strength of convective to the diffusive mechanism for respectively heat, mass, and cells. Therefore, it is a convenient way to predict the level of the heat, mass and cells transfer in the domain through these relations. The mean absolute error for each relation is presented in the last column. The correlations are captured by the PSO algorithm. The priority for the pertinent parameters is also obtained by the Machin learning method.

Table 7. The predictor correlations for Nusselt number with the effective range of parameters.

Effective range of parameters					**Parameters involved**	**Mean absolute error**
$0.1 \leq N_b \leq 100$	$0.1 \leq \lambda_1 \leq 100$	$0 \leq \phi_2 \leq 0.2$	$0.1 \leq Pr \leq 7.0$	$0 \leq \phi_1 \leq 0.2$		
$Nu = -6.668 + 9.531 \times {N_b}^{0.023}$					N_b	0.4680
$Nu = 3.38 + 0.934 \times {N_b}^{9.184} \times Re^{9.379}$					N_b, Re	0.4644
$Nu = 3.38 + 0.934 \times {N_b}^{1.783} \times Re^{1.978} \times Pr^{3.869}$					N_b, Re, Pr	0.4480
$Nu = 3.38 + 5.853 \times {N_b}^{0.377} \times Re^{5.894} \times Pr^{1.021} \times {\phi_1}^{6.874}$					N_b, Re, Pr, ϕ_1	0.4423
$Nu = 4.809 + 14.665 \times {N_b}^{2.938} \times Re^{3.459} \times Pr^{3.721} \times {\phi_1}^{5.15} \times {\phi_2}^{3.378}$					N_b, Re, Pr, ϕ_1	0.3715

Table 8. The predictor correlations for Sherwood number with the effective range of parameters.

Effective range of parameters	**Parameters involved**	

$0.1 \leq Sc \leq 5.0$	$0.1 \leq \gamma^* \leq 7.0$	$0.1 \leq N_b \leq 100$	$0.1 \leq Re \leq 100$		**Mean absolute error**
$Sh = 0.074 + 1.806 \times Sc^{0.22}$				Sc	0.1009
$Sh = 3.202 + 1.185 \times Sc^{0.236} \times Pr^{0.081}$				Sc , Pr	0.0951
$Sh = 1.162 + 0.146 \times Sc^{6.545} \times Pr^{1.452} \times {N_b}^{3.567}$				Sc , Pr , N_b	0.0812
$Sh = 1.160 + 0.825 \times Sc^{1.731} \times Pr^{2.874} \times {N_b}^{0.386} \times Re^{0.568}$				Sc , Pr , N_b, Re	0.0578

Table 9. The predictor correlations for density number of motile microorganisms number with the effective range of parameters.

Effective range of parameters				**Parameters involved**	**Mean absolute error**
$0.1 \leq Sc \leq 5.0$	$0.1 \leq \gamma^* \leq 7.0$	$0.1 \leq N_b \leq 100$	$0.1 \leq Re \leq 100$		
$Nn = 1.383 - 0.955 \times {L_b}^{-0.115}$				L_b	0.0613
$Nn = 1.042 + 0.0583 \times {L_b}^{0.19} \times Pr^{0.074}$				L_b , Pr	0.0573
$Nn = 0.154 + 0.725 \times {L_b}^{0.207} \times Pr^{0.206} \times \delta^{0.189}$				L_b , Pr , δ	0.0341
$Nn = 0.137 + 1.169 \times {L_b}^{1.779} \times Pr^{4.545} \times \delta^{1.816} \times Re^{1.771}$				L_b , Pr , δ, Re	0.0227

7. Conclusions

The transport processes in a hybrid nanofluid flow (Alumina-CNT nanotubes-water) over a cone merged in a porous medium were evaluated through an analytical-numerical investigation. The working fluid included motile alive cells to capture along with nanoparticles in a heat transferring medium. A large number of physical mechanisms including those of transport in porous media, nanofluid, mass transfer and bio-convection we present in the problem. This highly complicates the application of conventional approaches to simulation and analysis of the investigated system. As a remedy, machine learning was utilised to develop an intelligent predictor of the results and significantly broaden the parametric space. Further, machine learning was employed to derive correlations for the most dominant parameters, such as Nusselt and Sherwood number as well as density number of motile microorganisms. The key results are summarised as follows.

- Nusselt number increased for lower motile Lewis number, higher mixed convection parameter, bio Rayleigh number, Peclet number, and shape factor. However, the Nusselt number response to the motile Lewis number and mixed convection parameter were confined respectively by Peclet number increment and bio Rayleigh number increment.

- Sherwood number depicted a rising trend by decreasing volume fraction of nanotubes, Prandtl number, motile Lewis number, and intensifying mixed convection parameter and bio Rayleigh number. The effects of the mixed convection parameter was limited to high values for higher bio Rayleigh number.
- The density number of motile microorganisms was escalated as the volume fraction of the nanotubes rose.
- The mass concentration uniformity improved by increasing Reynolds number or mitigating Peclet number. Schmidt number and motile Lewis number variations elucidated no considerable change in the local mass content.
- Higher Prandtl number and lower Peclet number made a uniform motile microorganism distribution.
- The fluid temperature approached uniformity by degrading the mixed convection parameter, Reynolds number, and increasing Prandtl number. This was contributed by the negligible share of the volume fraction of Alumina and porosity.
- The non-dimensional solid temperature made a single-minimum distribution versus Biot number. Reynolds number while the ratio of fluid to solid thermal conductivity had no effect.

Finally, this work serves as a demonstrator of intelligent predictors built based on numerical simulations to massively reduce the computational burden of analyzing complex thermo-solutal problems.

References

(1) Chu, Y.M., ur Rahman, M., Khan, M.I., Kadry, S., Rehman, W.U. and Abdelmalek, Z. Heat transport and bio-convective nanomaterial flow of Walter's-B fluid containing gyrotactic microorganisms. Ain Shams Eng. J, **2021**, 12, 3071-3079. https://doi.org/10.1016/j.asej.2020.10.025.

(2) Bees, M.A. Advances in bioconvection. Annu. Rev. Fluid Mech. 2020, 52, 449-476.

(3) Khan, S.U., Al-Khaled, K. and Bhatti, M.M. Bioconvection analysis for flow of Oldroyd-B nanofluid configured by a convectively heated surface with partial slip effects. Surf. Interfaces, **2021**, 23, 100982.

(4) Taheri, M. and Bilgen, E. Thermo-bioconvection in a suspension of gravitactic micro-organisms in vertical cylinders. Int. J. Heat Mass Transfer, **2008**, 51, 3535-3547.

(5) Khan, S.U., Waqas, H., Muhammad, T., Imran, M. and Aly, S. Simultaneous effects of bioconvection and velocity slip in three-dimensional flow of Eyring-Powell nanofluid with Arrhenius activation energy and binary chemical reaction. Int. Commun. Heat Mass Transfer, **2020**, 117, 104738.

(6) Ullah, M.Z. and Jang, T.S. An efficient numerical scheme for analyzing bioconvection in von-Kármán flow of third-grade nanofluid with motile microorganisms. Alex. Eng. J. **2020**, 59, 2739-2752.

(7) Waqas, H., Khan, S.U., Hassan, M., Bhatti, M.M. and Imran, M. Analysis on the bioconvection flow of modified second-grade nanofluid containing gyrotactic microorganisms and nanoparticles. J. Mol. Liq. **2019**, 291, 111231.

(8) Song, Y.Q., Waqas, H., Al-Khaled, K., Farooq, U., Khan, S.U., Khan, M.I., Chu, Y.M. and Qayyum, S. Bioconvection analysis for Sutterby nanofluid over an axially stretched cylinder with melting heat transfer and variable thermal features: A Marangoni and solutal model. Alex. Eng. J. **2021**, 60, 4663-4675.

(9) Alshomrani, A.S., Ullah, M.Z. and Baleanu, D. Importance of multiple slips on bioconvection flow of cross nanofluid past a wedge with gyrotactic motile microorganisms. Case Stud. Therm. Eng. **2020**, 22, 100798.

(10) Belabid, J. and Allali, K. Thermo-bioconvection in horizontal porous annulus with the presence of phototactic microorganisms. Int J Eng Sci. **2019**, 140, 17-25.

(11) Uddin, M.J., Alginahi, Y., Bég, O.A. and Kabir, M.N. Numerical solutions for gyrotactic bioconvection in nanofluid-saturated porous media with Stefan blowing and multiple slip effects. Comput. Math. with Appl. **2016**, 72, 2562-2581.

(12) Devi, S. P. A. & Devi, S. S. U. Numerical investigation of hydromagnetic hybrid Cu- Al2O3/water nanofluid flow over a permeable stretching sheet with suction. Int. J. Nonlinear Sci. Numer. Simul. **2016**, 17, 249–257.

(13) Devi, S. S. U. & Devi, S. P. A. Numerical investigation of three-dimensional hybrid Cu–Al2O3/water nanofluid flow over a stretching sheet with effecting Lorentz force subject to Newtonian heating. Can. J. Phys. **2016**, 94, 490–496.

(14) Lund, L. A., Omar, Z., Raza, J. & Khan, I. Magnetohydrodynamic flow of Cu–Fe3O4/H2O hybrid nanofluid with effect of viscous dissipation: Dual similarity solutions. J. Therm. Anal. Calorim. **2020**, 143, 915-927, https://doi.org/10.1007/s10973-020-09602-1 (2020).

(15) Emami, R.Y., Siavashi, M. and Moghaddam, G.S. The effect of inclination angle and hot wall configuration on Cu-water nanofluid natural convection inside a porous square cavity. Adv. Powder Technol. **2018**, 29, 519-536.

(16) El-Shorbagy, M.A., Eslami, F., Ibrahim, M., Barnoon, P., Xia, W.F. and Toghraie, D. Numerical investigation of mixed convection of nanofluid flow in a trapezoidal channel with different aspect ratios in the presence of porous medium. Case Stud. Therm. Eng. **2021**, 25, 100977.

(17) Raizah, Z.A., Aly, A.M. and Ahmed, S.E. Natural convection flow of a nanofluid-filled V-shaped cavity saturated with a heterogeneous porous medium: Incompressible smoothed particle hydrodynamics analysis. Ain Shams Eng. J. **2021**, 12, 2033-2046.

(18) Cho, C.C. Effects of porous medium and wavy surface on heat transfer and entropy generation of Cu-water nanofluid natural convection in square cavity containing partially-heated surface. Int. Commun. Heat Mass Transfer, **2020**, 119, 104925.

(19) Cimpean, D.S., Sheremet, M.A. and Pop, I. Mixed convection of hybrid nanofluid in a porous trapezoidal chamber. Int. Commun. Heat Mass Transfer, **2020**, 116, 104627.

(20) Kadhim, H.T., Jabbar, F.A. and Rona, A. Cu-Al2O3 hybrid nanofluid natural convection in an inclined enclosure with wavy walls partially layered by porous medium. Int. J. Mech. Sci. **2020**, 186, 105889.

(21) Gholamalipour, P., Siavashi, M. and Doranehgard, M.H. Eccentricity effects of heat source inside a porous annulus on the natural convection heat transfer and entropy generation of Cu-water nanofluid. Int. Commun. Heat Mass Transfer, **2019**, 109, 104367.

(22) Khademi, R., Razminia, A. and Shiryaev, V.I. Conjugate-mixed convection of nanofluid flow over an inclined flat plate in porous media. Comput. Appl. Math, **2020**, 366, 124761.

(23) Moghadasi, H., Aminian, E., Saffari, H., Mahjoorghani, M. and Emamifar, A. Numerical analysis on laminar forced convection improvement of hybrid nanofluid within a U-bend pipe in porous media. Int. J. Mech. Sci. **2020**, 179, 105659.

(24) Waini, I., Ishak, A., Groşan, T. and Pop, I. Mixed convection of a hybrid nanofluid flow along a vertical surface embedded in a porous medium. Int. Commun. Heat Mass Transfer, **2020**, 114, 104565.

(25) Ahmed, S.E. Caputo fractional convective flow in an inclined wavy vented cavity filled with a porous medium using Al2O3-Cu hybrid nanofluids. Int. Commun. Heat Mass Transfer, **2020**, 116, 104690.

(26) Baïri, A. Using nanofluid saturated porous media to enhance free convective heat transfer around a spherical electronic device. Chinese J. Phys. **2021**, 70, 106-116.

(27) Sheikholeslami, M.. Influence of magnetic field on Al_2O_3-H_2O nanofluid forced convection heat transfer in a porous lid driven cavity with hot sphere obstacle by means of LBM. J. Mol. Liq. **2018**, 263, 472-488.

(28) Chamkha, A. J. Non-Darcy hydromagnetic free convection from a cone and a wedge in porous media. Int. Commun. Heat Mass Transfer. **1996**, 23, 875-887.

(29) Chamkha, A. J., & Al-Mudhaf, A. Unsteady heat and mass transfer from a rotating vertical cone with a magnetic field and heat generation or absorption effects. Int. J. Therm. Sci. **2005**, 44, 267-276.

(30) Chamkha, A. J. Coupled heat and mass transfer by natural convection about a truncated cone in the presence of magnetic field and radiation effects. Numer. Heat Transf.; A: Appl. **2001**, 39, 511-530.

(31) Takhar, H. S., Chamkha, A. J., & Nath, G. Unsteady mixed convection flow from a rotating vertical cone with a magnetic field. Heat Mass Transfer. **2003**, 39, 297-304.

(32) Takhar, H. S., Chamkha, A. J., & Nath, G. Combined heat and mass transfer along a vertical moving cylinder with a free stream. Heat Mass Transfer. **2000**, 36, 237-246.

(33) Platt, J. R. Bioconvection Patterns in Cultures of Free-Swimming Organisms. Science, **1961**, 133, 1766-1767.

(34) Abe, T., Nakamura, S., & Kudo, S. Bioconvection induced by bacterial chemotaxis in a capillary assay. Biochem. Biophys. Res. Commun. **2017**, 483, 277-282.

(35) Kuznetsov, A. V. The onset of thermo-bioconvection in a shallow fluid saturated porous layer heated from below in a suspension of oxytactic microorganisms. Eur. J. Mech. B Fluids, **2006**, 25, 223-233.

(36) Kuznetsov, A. V. The onset of nanofluid bioconvection in a suspension containing both nanoparticles and gyrotactic microorganisms. Int. Commun. Heat Mass Transfer, **2010**, 37, 1421-1425.

(37) Kuznetsov, A. V. Nanofluid bioconvection in water-based suspensions containing nanoparticles and oxytactic microorganisms: oscillatory instability. Nanoscale Res. Lett. **2011**, 6, 100.

(38) Saini, S., & Sharma, Y. D. A bio-thermal convection in water-based nanofluid containing gyrotactic microorganisms: effect of vertical throughflow. J. Appl. Fluid Mech. **2018**, 11, 895-903.

(39) Saini, S., & Sharma, Y. D. Analysis of onset of bio-thermal convection in a fluid containing gravitactic microorganisms by the energy method. Chinese J. Phys. **2018**, 56, 2031-2038.

(40) Saini, S., & Sharma, Y. D. Numerical study of nanofluid thermo-bioconvection containing gravitactic microorganisms in porous media: Effect of vertical throughflow. Adv. Powder Technol. **2018**, 29, 2725-2732.

(41) Xu, H. Lie group analysis of a nanofluid bioconvection flow past a vertical flat surface with an outer power-law stream. J. Heat Transfer, **2015**, 137, 041101-1.

(42) Zaimi, K., Ishak, A., & Pop, I. Stagnation-point flow toward a stretching/shrinking sheet in a nanofluid containing both nanoparticles and gyrotactic microorganisms. J. Heat Transfer, **2014**, 136, 041705.

(43) Xu, H., & Pop, I. Fully developed mixed convection flow in a horizontal channel filled by a nanofluid containing both nanoparticles and gyrotactic microorganisms. Eur. J. Mech. B Fluids, **2014**, 46, 37-45.

(44) Bég, O. A., Uddin, M. J., & Khan, W. A. Bioconvective non-Newtonian nanofluid transport in porous media containing micro-organisms in a moving free stream. J Mech Med Biol. **2015**, 15, 1550071.

(45) Kumar, R., Sood, S., Raju, C.S.K. and Shehzad, S.A. Hydromagnetic unsteady slip stagnation flow of nanofluid with suspension of mixed bio-convection. PROPULS POWER RES., **2019**, 8, 362-372.

(46) Pan, Y. and Zhang, L. Roles of artificial intelligence in construction engineering and management: A critical review and future trends. Autom. Constr. **2021**, 122, 103517.

(47) Mesgarpour, M., Abad, J. M. N., Alizadeh, R., Wongwises, S., Doranehgard, M. H., Ghaderi, S., & Karimi, N. Prediction of the spread of Corona-virus carrying droplets in a bus-A computational based artificial intelligence approach. J. Hazard. Mater. **2021**, 413, 125358.

(48) Alizadeh, R., Abad, J. M. N., Ameri, A., Mohebbi, M. R., Mehdizadeh, A., Zhao, D., & Karimi, N. A machine learning approach to the prediction of transport and thermodynamic processes in multiphysics systems-heat transfer in a hybrid nanofluid flow in porous media. J. Taiwan Inst. Chem. Engrs. **2021**, 124, 290-306. https://doi.org/10.1016/j.jtice.2021.03.043

(49) Panwar, Vishwanath, Seshu Kumar Vandrangi, and Sampath Emani. "Artificial intelligence-based computational fluid dynamics approaches." In *Hybrid Computational Intelligence*, pp. 173-190. Academic Press, **2020**.

(50) Brunton, S.L., Hemati, M.S. & Taira, K. Special issue on machine learning and data-driven methods in fluid dynamics. Theor. Comput. Fluid Dyn. **2020**, 34, 333–337. https://doi.org/10.1007/s00162-020-00542-y

(51) Alizadeh, R., Mohebbi Najm Abad, J., Fattahi, A., Mohebbi, M. R., Doranehgard, M. H., Li, L. K., & Karimi, N. A machine learning approach to predicting the heat convection and thermodynamics of an external flow of hybrid nanofluid. J Energy Resour Technol. **2021**, 143, 070908-1.

(52) Alizadeh, R., Mohebbi Najm Abad, J., Fattahi, A., Alhajri, E. S., & Karimi, N. Application of Machine Learning to Investigation of Heat and Mass Transfer Over a Cylinder Surrounded by Porous Media-The Radial Basic Function Network. J Energy Resour Technol. **2020**, 142, 112109-1.

(53) Abad, J. M. N., Alizadeh, R., Fattahi, A., Doranehgard, M. H., Alhajri, E., & Karimi, N. Analysis of transport processes in a reacting flow of hybrid nanofluid around a bluff-body embedded in porous media using artificial neural network and particle swarm optimization. J. Mol. Liq. **2020**, 313, 113492.

(54) Hassanpour, M., Vaferi, B. and Masoumi, M.E. Estimation of pool boiling heat transfer coefficient of alumina water-based nanofluids by various artificial intelligence (AI) approaches. Appl. Therm. Eng. **2018**, 128, 1208-1222.

(55) Kumra, A., Rawal, N. and Samui, P. Prediction of heat transfer rate of a Wire-on-Tube type heat exchanger: An Artificial Intelligence approach. Procedia Eng. **2013**, 64, 74-83.

(56) Kumar, R., Bhattacharyya, A., Seth, G. S., & Chamkha, A. J. Transportation of magnetite nanofluid flow and heat transfer over a rotating porous disk with Arrhenius activation energy: Fourth order Noumerov's method. Chin. J. Phys. **2021**, 69, 172-185.

(57) Sadeghi, M. S., Anadalibkhah, N., Ghasemiasl, R., Armaghani, T., Dogonchi, A. S., Chamkha, A. J. & Asadi, A. On the natural convection of nanofluids in diverse shapes of enclosures: an exhaustive review. J. Therm. Anal. Calorim. **2020**, 1-22. https://doi.org/10.1007/s10973-020-10222-y.

(58) Reddy, P. S., Sreedevi, P., & Chamkha, A. J. MHD boundary layer flow, heat and mass transfer analysis over a rotating disk through porous medium saturated by Cu-water and Ag-water nanofluid with chemical reaction. Powder Technol. **2017**, 307, 46-55.

(59) Ghalambaz, M., Behseresht, A., Behseresht, J., & Chamkha, A. Effects of nanoparticles diameter and concentration on natural convection of the Al_2O_3–water nanofluids considering variable thermal conductivity around a vertical cone in porous media. Adv. Powder Technol. **2015**, 26, 224-235.

(60) Rasool, G., Zhang, T., Chamkha, A. J., Shafiq, A., Tlili, I., & Shahzadi, G. (2020). Entropy generation and consequences of binary chemical reaction on MHD Darcy–Forchheimer Williamson nanofluid flow over non-linearly stretching surface. Entropy, **2020**, 22, 18.

(61) Khan, M. R., Pan, K., Khan, A. U. & Nadeem, S. Dual solutions for mixed convection flow of $SiO_2-Al_2O_3$/water hybrid nanofluid near the stagnation point over a curved surface. Phys. A Stat. Mech. its Appl. **2019**, 547, 123959. https://doi.org/10.1016/j.physa.2019.12395 (2020).

(62) Zadeh, S.M.H., Mehryan, S.A.M., Sheremet, M.A., Izadi, M. and Ghodrat, M. Numerical study of mixed bio-convection associated with a micropolar fluid. Therm. Sci. Eng. Prog. **2020**, 18, 100539.

(63) Khan, W. A., Khan, Z. H., & Rahi, M. Fluid flow and heat transfer of carbon nanotubes along a flat plate with Navier slip boundary. Appl. Nanosci. **2014**, 4, 633-641.

(64) Gorla, R.S.R. Heat transfer in an axisymmetric stagnation flow on a cylinder. Appl. Sci. Res. **1976**, 32, 541-553.

(65) Hassoun, M.H Fundamentals of artificial neural networks. MIT press, Cambridge MA, **1995**, 42, 1322.

(66) Alanis, A.Y.; Arana-Daniel, N. and Lopez-Franco, C. eds. Artificial Neural Networks for Engineering Applications. Academic Press, Cambridge MA, **2019**, 176.

Table of Content

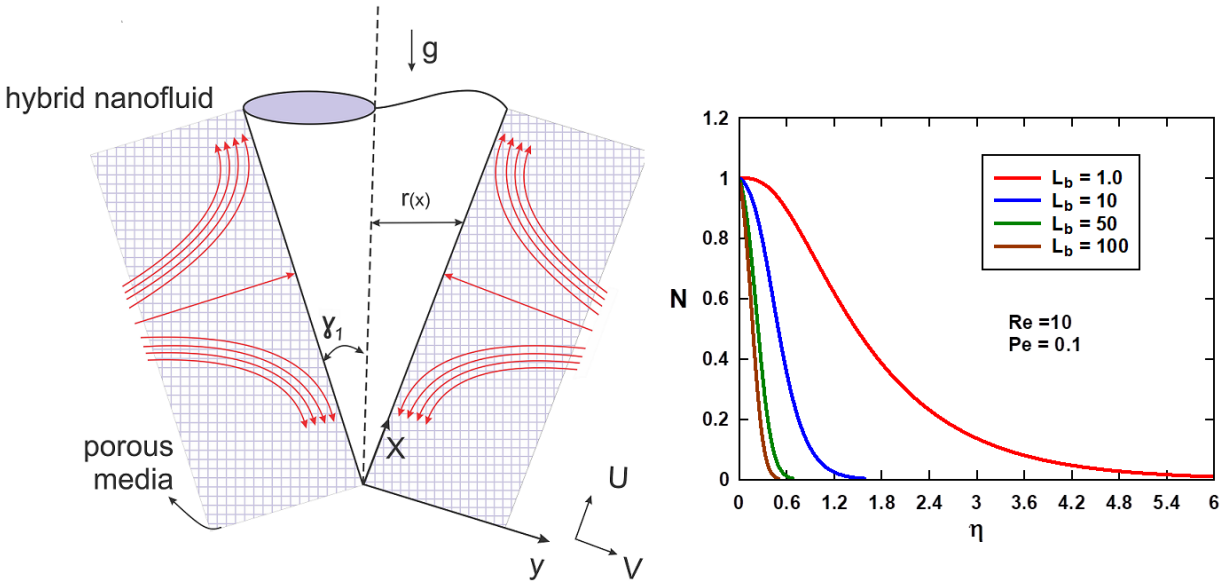

Variation of N with respect to η at different values of bio-convection Lewis number.